

# Cell Surface SARS-CoV-2 Nucleocapsid Protein Modulates Innate and Adaptive Immunity

Jonathan Yewdell (✉ [jyewdell@nih.gov](mailto:jyewdell@nih.gov))

National Institutes of Health <https://orcid.org/0000-0002-3826-1906>

Alberto Lopez-Munoz

National Institutes of Health

Ivan Kosik

Laboratory of Viral Diseases

Jaroslav Holly

National Institutes of Health

---

Biological Sciences - Article

Keywords:

**Posted Date:** December 13th, 2021

**DOI:** <https://doi.org/10.21203/rs.3.rs-1162804/v1>

**License:** © ⓘ This work is licensed under a Creative Commons Attribution 4.0 International License.

[Read Full License](#)

---

1 **Cell Surface SARS-CoV-2 Nucleocapsid Protein Modulates Innate and Adaptive Immunity**

2

3 Alberto Domingo López-Muñoz, Ivan Kosik, Jaroslav Holly, Jonathan W. Yewdell\*

4

5 Cellular Biology Section, Laboratory of Viral Diseases, NIAID (NIH), Bethesda, Maryland,  
6 United States

7

8 \* Corresponding author

9 E-mail: [jyewdell@nih.gov](mailto:jyewdell@nih.gov)

10

11

12

13

14

15

16

17

18

19 **SARS-CoV-2 Cell Surface N Immune Interactions**

20

21

22

23

## 24 **ABSTRACT**

25 SARS-CoV-2 nucleocapsid protein (N) induces strong antibody and T cell responses. Although  
26 considered to be localized in the cytosol, we readily detect N on the surface of live cells. N released  
27 by SARS-CoV-2 infected cells or N-expressing transfected cells binds to neighboring cells by  
28 electrostatic high-affinity binding to heparan sulfate and heparin, but not other sulfated  
29 glycosaminoglycans. N binds with high affinity to 11 human chemokines, including CXCL12 $\beta$ ,  
30 whose chemotaxis of leukocytes is inhibited by N from SARS-CoV-2, SARS-CoV-1, and MERS  
31 CoV. Anti-N Abs bound to the surface of N expressing cells activate Fc receptor-expressing cells.  
32 Our findings indicate that cell surface N manipulates innate immunity by sequestering chemokines  
33 and can be targeted by Fc expressing innate immune cells. This, in combination with its conserved  
34 antigenicity among human CoVs, advances its candidacy for vaccines that induce cross-reactive  
35 B and T cell immunity to SARS-CoV-2 variants and other human CoVs, including novel zoonotic  
36 strains.

37

## 38 **INTRODUCTION**

39 Despite the unprecedented expeditious development and deployment of highly effective vaccines,  
40 the rapid selection of SARS Coronavirus (CoV) 2 (SARS-CoV-2) spike glycoprotein (S) antibody  
41 (Ab) escape mutants threatens to delay the return to pre-pandemic conditions. To broaden  
42 vaccination and reduce SARS-CoV-2 related acute and chronic disease, it is crucial to improve  
43 our knowledge of innate and adaptive immunity to CoVs.

44 CoVs encode four major structural proteins. S, membrane (M), and envelope (E) proteins are  
45 localized in the viral surface envelope. N binds to viral RNA through electrostatic interactions,  
46 forming cytoplasmic helical nucleocapsids that associate with M to enable virus budding into early  
47 secretory compartments. As the most abundantly expressed SARS-CoV-2 protein, N induces  
48 strong Ab and T<sub>CD8+</sub> immune responses<sup>1,2</sup>. Although CoV N is widely considered to be strictly  
49 localized in the cytoplasm, cell surface expression of RNA viruses N is more the rule than the  
50 exception. Early studies with monoclonal Abs (mAbs) reported surface expression of influenza A  
51 and vesicular stomatitis virus N<sup>3,4</sup>. Influenza N is a target for Ab-complement-mediated cell lysis<sup>3</sup>,  
52 Ab redirected T cell lysis<sup>5</sup>, and is targeted by protective Abs in mice<sup>6</sup>. N and N-like RNA genome  
53 binding proteins are expressed on the surface of cells infected with other human viruses, including  
54 measles<sup>7</sup>, respiratory syncytial<sup>8</sup>, lymphocytic choriomeningitis<sup>9</sup>, and human immunodeficiency  
55 virus<sup>10</sup>.

56 Here, we examine the expression of human CoV N on the cell surface and its participation in innate  
57 and adaptive immunity.

58

## 59 **RESULTS**

### 60 **SARS-CoV-2 N is robustly expressed on the infected cell surface**

61 We examined cell surface expression of SARS-CoV-2 N by imaging Vero cells 24 h post-infection  
62 (hpi) with wild-type (wt) or a recombinant SARS-CoV-2 expressing eGFP (SARS-CoV-2\_eGFP).  
63 To exclusively detect cell surface N, we incubated live cells with primary and fluorophore-  
64 conjugated secondary antibodies at 4°C prior to fixation and mounting for confocal imaging. This  
65 revealed clear surface N staining over mock-infected (mock) background levels, using S or eGFP

66 as markers of infected cells (Fig. 1a (maximum intensity projection images of z-stack). We  
67 similarly found N on the surface of BHK-21\_humanACE2(hACE2), Caco-2, Calu-3, CHO-  
68 K1\_hACE2, and HEK293-FT\_hACE2 cells infected with wt or eGFP SARS-CoV-2 at 24 hpi  
69 (Extended Data Fig. 1, 2). Depending on the cell type, we observed a variable degree of  
70 colocalization between N and S, particularly remarkable in Vero (Fig. 1a), Calu-3, CHO-  
71 K1\_hACE2, and HEK293-FT\_hACE2 cells (Extended Data Fig. 1). We noted a dramatic syncytia  
72 formation in hACE2 overexpressing BHK-21\_hACE2 and HEK293-FT\_hACE2 cells as reported  
73 <sup>11</sup>.

74 To measure N surface expression more quantitatively, we performed flow cytometry analyses of  
75 live infected cells 24 hpi. Surface N was detected on a subpopulation of S or eGFP expressing cells  
76 for each of the seven cell types examined (Fig. 1b, Extended Data Fig. 1-3). N was also detected  
77 on the surface of live cells infected with Alpha (B.1.1.7), Beta (B.1.351) and Delta (B.1.617.2)  
78 SARS-CoV-2 variants (Extended Data Fig. 4). Via flow cytometry, we determined the kinetics of  
79 N expression on the surface of Vero (Fig. 1c-d), BHK-21\_hACE2, and A549\_hACE2 cells  
80 (Extended Data Fig. 5). As early as 8 hpi, we observed a significant surface signal for N protein in  
81 live Vero and BHK-21\_hACE2 infected cells, while it took slightly longer (12 hpi) for  
82 A549\_hACE2 cells (Extended Data Fig. 5). Notably, depending on cell type and marker of  
83 infection (S vs. eGFP) we detected cells expressing N but not S or eGFP on a fraction of cells,  
84 ranging from less than 1% to 43% (Extended Data Fig. 1, 2). This is consistent with several  
85 mechanisms acting alone or in combination: differential expression of SARS-CoV-2 gene products  
86 in individual cells <sup>12</sup>, complete retention of S in the secretory pathway <sup>13</sup>, and transfer of N from  
87 infected to non-infected cells.

88 To determine whether N cell surface expression requires other SARS-CoV-2 gene products, we  
89 transfected cells with an expression plasmid encoding N. Staining of live BHK-21, CHO-K1 or  
90 HEK293-FT cells transfectants revealed up to 7-fold more N mAb binding over background levels  
91 obtained with cells transfected with a control plasmid expressing eGFP (Fig. 2a). N-surface  
92 expression increased between 24 and 72 h post-transfection, providing further evidence for the  
93 specificity of staining, and demonstrating that cell surface expression is an intrinsic property of  
94 biosynthesized N.

### 95 **Exogenous N binds to cells**

96 To examine whether N surface expression requires its synthesis in the cell, we incubated BHK-21,  
97 CHO-K1, or HEK293-FT cells with exogenous purified recombinant N (rN) for 15 min at 37 °C  
98 resulted in. This resulted in strong flow cytometry staining (2-log shift) with anti-N mAbs relative  
99 to control cells incubated with an irrelevant protein (Fig. 2b).

100 N interacts with negatively charged viral RNA through highly positively charged RNA-binding  
101 domains<sup>14,15</sup>. We examined charge-based N binding to the cell surface by treating rN coated cells  
102 with polybrene, a cationic polymer that neutralizes surface electrostatic charges. Flow cytometric  
103 analysis showed that polybrene decreases rN bound to live BHK-21, CHO-K1, and HEK293-FT  
104 cells to similar levels, with the magnitude of the effect proportional to the amount of bound N (Fig.  
105 2c).

106 For most mammalian cells, glycosaminoglycans (GAGs) are the major negatively charged  
107 molecule on the plasma membrane<sup>16</sup>. To assess the contribution of GAGs to N cell surface binding,  
108 we used a panel of GAG-deficient CHO cells<sup>17</sup>. Each of the GAG-deficient cell lines tested failed  
109 to bind rN over levels observed with recombinant GFP (Fig. 2d). The panel included cells with

110 complete absence of GAGs (CHO-pgsA-745, HO-pgsB-618), and cells with defects in  
111 synthesizing heparan sulfate and heparin but no other GAGs (CHO-pgsD-677, CHO-pgsE-606).  
112 Consistent with these findings, treating Vero, BHK-21, CHO-K1, or HEK293-FT cells with  
113 heparinase I, II, and III in combination, to depolymerize heparan sulfate/heparin polysaccharide  
114 chains to disaccharides, cells dramatically reduced binding of exogenous rN (Fig. 2e, Extended  
115 Data Fig. 6c). We directly confirmed N binding to heparin by using bilayer interferometry (BLI),  
116 where we directly demonstrate N specific nanomolar affinity binding to heparan sulfate and  
117 heparin, but not to other sulfated GAGs (Fig. 2f, Extended Data Fig. 6d, e).

118 Together, these findings indicate that N binds to the cell surface by interacting with heparan sulfate  
119 and heparin in a charge-dependent manner.

### 120 **N is transferred from expressing to non-expressing cells**

121 In SARS-CoV-2 24 hpi immunofluorescence and flow cytometry experiments (Fig. 1a, b,  
122 Extended Data Fig. 1, 2), we observed cells expressing N but not S or GFP as early as 8 and 12  
123 hpi (Extended Data Fig. 5), with increasing numbers of cells over time after infection (Extended  
124 Data Fig. 7). To determine whether N can be transferred from infected to non-infected cells, we  
125 added SARS-CoV-2 to a co-culture of infectable (hACE2 expressing) and non-infectable (non-  
126 hACE2 expressing) CHO-K1 cells (we confirmed that hACE2 is required for infecting CHO cells  
127 with SARS-CoV-2, see Supplementary Fig. 1a). We pre-stained non-infectable cells with  
128 CellTrace™ Violet to enable unambiguous flow identification after co-culture (Supplementary  
129 Fig. 1b). Remarkably, co-cultured non-ACE2 expressing uninfected CHO-K1 cells (also  
130 confirmed by the absence of S expression) have a higher cell surface N signal than infected cells  
131 (Fig. 3a, Supplementary Fig. 1c). N transfer from infected cells required GAG expression on  
132 uninfected cells, as shown by near background staining by GAG-deficient CHO cells (Fig. 3b, c,  
133 Supplementary Fig. 1d, e). N is also transferred from HEK293-FT or BHK-21 cells transiently  
134 expressing N from a transgene to co-cultured un-transfected cells (Fig. 3d).

135 Based on these findings, we conclude that N protein synthesis leads to its release from cells and  
136 its robust transfer to non-synthesizing cells, where it is retained by binding heparin/heparan sulfate.

### 137 **SARS-CoV-2 N inhibits chemokine function but enables Ab based immune cell activation**

138 The robust expression of N on the surface of infected and surrounding cells suggests a significant  
139 evolutionary function. SARS-CoV-2, like most viruses, induces the release of pro-inflammatory  
140 cytokines by infected cells. Could N interfere with this signaling? We examined the ability of  
141 immobilized N to interact with 64 human cytokines by BLI. Remarkably N bound CCL5, CCL11,  
142 CCL21, CCL26, CCL28, CXCL4, CXCL9, CXCL10, CXCL11, CXCL12 $\beta$ , and CXCL14  
143 chemokines with micromolar to nanomolar affinities (Fig. 4a, Extended Data Fig. 8). By contrast,  
144 none of the other SARS-CoV-2 immobilized structural (S, M, E) or non-structural (ORFs 3a, 3b,  
145 6, 7a, 7b, 8, 9b, 9c, and 10) proteins tested interacted with any of the cytokines in the panel with  
146 affinities higher than that observed for immobilized GFP (Extended Data Fig. 9a). Kinetic curves  
147 of N binding to each chemokine were biphasic, deviating from first-order binding (1:1) and  
148 consistent with heterogeneous binding (Extended Data Fig. 8).

149 Chemokine function is based on interaction with both surface GAGs and their specific receptors  
150 located in the surface of leukocytes. We found that blocking the GAG-binding domain of  
151 chemokines by increasing concentrations of heparan sulfate (from bovine kidney) and chondroitin

152 sulfate A and B, N binding to its subset of chemokines was abrogated (Extended Data Fig. 10).  
153 This indicates that N binds to chemokines through their GAG-binding domain.

154 What is the functional relevance of N-chemokine interactions? Transwell chemotaxis experiments  
155 with monocyte-like cells (MonoMac-1), T lymphocyte-like cells (MOLT-4), and human healthy  
156 donor PBMCs revealed that rN blocked CXCL12 $\beta$ -induced chemotaxis in a concentration-  
157 dependent manner (Fig. 4b). While rN from different vendors showed comparable results  
158 inhibiting CXCL12 $\beta$ -mediated induction of migration of MonoMac-1 cells, the S1 protein (subunit  
159 1 of the S protein, containing the receptor-binding domain) had no inhibitory effect on CXCL12 $\beta$ -  
160 induced chemotaxis (Supplementary Fig. 2). Extending these findings, rN from both SARS-CoV-  
161 1 and MERS-CoV also inhibited CXCL12 $\beta$  induced migration of MonoMac-1 cells (Fig. 4c).

162 mAbs to mouse CoV N have been reported to exert anti-viral activity *in vitro* (with complement)  
163 and *in vivo*<sup>18,19</sup>. To examine their potential as a target for antibody dependent cellular cytotoxicity  
164 (ADCC), we used Fc $\gamma$ RIIIa receptor-expressing Jurkat reporter cells as a surrogate for ADCC  
165 effector cell recognition of anti-N mAb coated SARS-CoV-2 infected cells. Vero and BHK-  
166 21\_hACE2 SARS-CoV-2 infected cells activated reporter cells in an anti-N mAb concentration-  
167 dependent manner (Fig. 4d). Activation was not observed in the absence of infection or with a  
168 control human mAb with the same heavy chain.

169 Taken together, these findings indicate that N protein from each of the highly pathogenic human  
170 CoVs blocks chemokine function. This is consistent with the possibility that cell surface N blocks  
171 chemokine function *in vivo*, facilitating viral replication and transmission. Conversely, we also  
172 show that cell surface N is a potential target for ADCC, which potentially contributes to limiting  
173 viral replication and transmission.

174

## 175 **DISCUSSION**

176 Here, we show that N synthesized during SARS-CoV-2 infection or from a transfected cDNA is  
177 expressed on the surface of both N synthesizing cells and neighboring cells. N binding to the cell  
178 surface is based on specific association with heparan sulfate and heparin. The most parsimonious  
179 explanation for these findings is that N is released from cells and binds to both producing and  
180 bystander cells from liquid phase. Remarkably, based on the flow cytometry, levels of N on SARS-  
181 CoV-2 infected cells equals or exceeds cell surface S on all but one of the seven cell types  
182 examined. This, in part is due to the retention of a substantial fraction of S in the early secretory  
183 pathway but also reflects a robust amount of cell surface N, likely in the range of 10<sup>4</sup>-10<sup>5</sup> copies  
184 per cell.

185 The mechanism underlying N secretion remains to be established. N has two potential sites for  
186 addition of N-linked oligosaccharides in the secretory pathway that are glycosylated and readily  
187 detected when N is targeted to the ER with an artificial N-terminal signal sequence<sup>20</sup>. Without a  
188 signal sequence, N is not glycosylated. This indicates that, as with other viral nucleic acid-binding  
189 proteins (*e.g.*, SV40 T antigen, influenza virus N), SARS-CoV-2 N is likely secreted through a  
190 non-canonical secretory pathway, possibly one of the three defined pathways that bypass insertion  
191 into the ER<sup>21</sup>. Interestingly, like N, several proteins non-canonically exported to the cell surface  
192 (HIV Tat, FGF2, and tau) bind heparan sulfate, which has been shown to be involved in traversing  
193 the plasma membrane<sup>22</sup>. It will be interesting to examine the extent to which cell surface export of

194 N and other viral RNA binding proteins, as well as their cell surface binding, is based on heparan  
195 sulfate association.

196 N is typically the most abundantly expressed SARS-CoV-2 protein, and its transfer to non-infected  
197 cells potentially amplifies its contributions to viral fitness. The remarkable ability of cell surface  
198 N to bind chemokines and block chemotaxis of immune effector cells offers an evolutionary  
199 explanation for its cellular export and binding to infected and neighboring uninfected cells. Like  
200 N, chemokines are immobilized on source cells and their neighbors by binding to GAGs. A number  
201 of viruses are known to express chemokine-binding proteins, which modulate chemokine activity  
202 by interacting with the GAG- or receptor-binding domain of chemokines, or both<sup>23,24</sup>. Our findings  
203 establish SARS-CoV-2 N as the first CoV chemokine binding protein, one with a remarkably high  
204 affinity (nanomolar range) for multiple chemokines.

205 The binding of N to heparin, which limits coagulation at inflammation sites, suggests a possible  
206 role for secreted N in promoting COVID-associated clotting abnormalities. N is present in intestine  
207 and lungs from recovered and fatal COVID-19 patients, respectively, while virus-like particles are  
208 rarely detected<sup>25,26</sup>, consistent with this intriguing possibility as well as a role in the chronic low  
209 level inflammation that causes “long COVID-19” symptoms.

210 The remarkable efficacy of spike only-vaccines demonstrates that antibodies to N are not required  
211 for COVID-19 protection. SARS-CoV-2 induces a robust anti-N Ab response, in part likely due  
212 to cross-reaction with memory B cells induced by seasonal CoV infections. These Abs may reduce  
213 SARS-CoV-2 disease in naïve individuals since we establish N as a potential target for antibody-  
214 mediated effector functions, including complement and NK cell-mediated lysis of infected cells.  
215 Abs, therefore may play an unexpected role in protection to SARS-CoV-2 infection afforded by  
216 immunization with N-expressing vectors presumed to function via induction of N-specific T  
217 cells<sup>27-30</sup>. N is an attractive vaccine target due to its strong immunogenicity and much lower  
218 antigenic drift than spike. This may be particularly relevant given the remarkable capacity of  
219 SARS-CoV-2 to acquire amino changes in S as illustrated by the recent introduction of the omicron  
220 variant with over thirty non-synonymous mutations in S.

221 In summary, our findings demonstrate unexpected roles for N in innate and adaptive immunity to  
222 SARS-CoV-2 and other human CoVs that may contribute to both pathogenesis and protection, and  
223 support N as an Ab and T cell target for future “universal” vaccines that provide broad protection  
224 against both future strains of SARS-CoV-2 as well as other human CoVs.

225

## 226 **METHODS**

### 227 **Cells**

228 Vero cells (# CCL-81), BHK-21 (# CCL-10), Caco-2 (# HTB-37), Calu-3 (# HTB-55), CHO-K1  
229 (# CCL-61), CHO-pgsA-745 (# CRL-2242), CHO-pgsB-618 (# CRL-2241), CHO-pgsD-677 (#  
230 CRL-2244), CHO-pgsE-606 (# CRL-2246), HEK293-FT (# CRL-11268), A549 (# CCL-185) and  
231 MOLT-4 (# CRL-1582) cells were from the American Type Culture Collection (ATCC).  
232 MonoMac-1 cells (# ACC 252) were from the DSMZ-German Collection of Microorganisms and  
233 Cell Cultures. PBMCs were obtained from a healthy donor with informed consent, at the  
234 Department of Transfusion Medicine (NIH). Vero, BHK-21, Caco-2, Calu-3 and HEK293-FT cells  
235 were grown in DMEM with GlutaMAX (Thermo Fisher # 10566016). CHO-K1, CHO-pgsA-745,  
236 CHO-pgsB-618, CHO-pgsD-677, CHO-pgsE-606 and A549 cells were grown in F-12K medium  
237 (Thermo Fisher # 21127022). PBMCs, MOLT-4 and MonoMac-1 cells were grown in RPMI 1640  
238 (Thermo Fisher # 11875119). BHK-21\_hACE2, CHO-K1\_hACE2, HEK293-FT\_hACE2 and  
239 A549\_hACE2 cells were grown in their correspondent medium with 250-500 µg/ml of blasticidin  
240 (Invivogen # ant-bl-1). All cell media were supplemented with 8% (v/v) not heat inactivated FBS  
241 (Hyclone # SH30071.03), but Caco-2 with 20%, and cells were grown cultured at 37° C with 5%  
242 CO<sub>2</sub> in sterile flasks. Cells were passaged at ~80-90% confluence and seeded as explained for each  
243 individual assays.

### 244 **SARS-CoV-2 stock preparation**

245 SARS-CoV-2 (isolate USA-WA1/2020, # NR-52281), SARS-CoV-2\_eGFP (# NR-54002) and the  
246 Alpha variant (B.1.1.7, # NR-54000) were obtained from BEI resources. The Beta (B.1.351) and  
247 Delta variants (B.1.617.2) were obtained from Andrew Pekosz (Johns Hopkins University, US).  
248 Viruses were propagated by the NIAID SARS-CoV-2 Virology Core Laboratory under BSL-3  
249 conditions using Vero (CCL-81) or Vero overexpressing human TMPRSS2 cells, cultured in  
250 DMEM supplemented with GlutaMAX, 2% FBS, penicillin, streptomycin, and fungizone. Virus  
251 stocks were deep-sequenced and subjected to minor variants analysis by the NIAID SARS-CoV-  
252 2 Virology Core Laboratory. The TCID<sub>50</sub> and PFU of virus in clarified culture medium was  
253 determined on Vero cells after staining with crystal violet. SARS-CoV-2 infections were  
254 performed in the NIAID SARS-CoV-2 Virology Core BSL3 laboratory strictly adhering to its  
255 standard operative procedures.

### 256 **Generating mutant cell lines constitutively expressing hACE2**

257 The Sleeping Beauty transposase system was used for the generation of BHK-21\_hACE2, CHO-  
258 K1\_hACE2, HEK293-FT\_hACE2 and A549\_hACE2 cells as previously described<sup>31,32</sup>. In brief,  
259 a semi-confluent 60 mm plate was seeded with each cell line and co-transfected with 0.5 µg of  
260 pCMV(CAT)T7-SB100 (Transposase vector, Addgene # 34879) and 5 µg of pSBbi-Bla hACE2  
261 (Transposon vector), using TransIT-LT1 Transfection Reagent (Mirus Bio), following  
262 manufacturer instructions. After 24 h, cells were transferred to a T-75 flask and selected with 250-  
263 500 µg/ml of blasticidin for two weeks. The surface expression of hACE2 was confirmed by flow  
264 cytometry using anti-human ACE2 AlexaFluor 647-conjugated Ab (R&D Systems, # FAB9332R).  
265 The expression was further confirmed by immunoblot using hACE2 Ab (Cell Signaling  
266 Technology, # 4355). The open reading frame of hACE2 (kindly provided by Sonja Best from  
267 NIAID/NIH) was cloned into pSBbi-Bla vector (Addgene # 60526) as described<sup>31</sup>.

### 268 **Antibodies**

269 Previously published Ab VH and VL amino acid sequences against SARS-CoV-2 N (# N18<sup>33</sup>) and  
270 SARS-CoV-2 S (# H4<sup>34</sup>) were commercially synthesized, cloned into a human IgG1 vector  
271 backbone, produced and purified (Synbio Technologies). A 100 µg aliquot of anti-SARS-CoV-2  
272 N human mAb was conjugated with Alexa Fluor<sup>®</sup> 647 Lightning-Link<sup>®</sup> Conjugation Kit (Abcam  
273 # ab269823), while 100 µg of anti-SARS-CoV-2 S were conjugated with Alexa Fluor<sup>®</sup> 488  
274 Lightning-Link<sup>®</sup> Conjugation Kit (Abcam # ab236553). Each experiment was repeated with  
275 similar results using anti-SARS-CoV-2 N rabbit polyclonal Ab (GeneTex # GTX135357) and anti-  
276 SARS-CoV-2 S rabbit polyclonal Ab (ProSci # 3525). Goat anti-mouse IgG Alexa Fluor 488-  
277 conjugated (Thermo # A-11001) or 647 (# A-21235), goat anti-rabbit IgG Alexa Fluor 488 (# A-  
278 11008) or 647 (# A-21245), and Goat anti-human IgG Alexa Fluor 488 (# A-11013) or 647 (# A-  
279 21445) were used as a secondary Abs.

280 The SARS-CoV-2 S stabilized (S<sup>st</sup>) sequence<sup>35</sup> (R710G, R711S, R713S, K1014P, V1015P) was  
281 commercially cloned into a mammalian expression vector, produced and purified (GenScript  
282 Biotech). Mouse polyclonal anti-SARS-CoV-2 S<sup>st</sup> serum was produced as followed: 8-to-12-week  
283 C57B6 mice (Taconic Farms Inc) were immunized with 4 µg of S<sup>st</sup> diluted in DPBS, adjuvanted  
284 by TiterMax<sup>®</sup> Gold (MilliporeSigma # T2684) (2:1) in 50 µl volume via intramuscular injections.  
285 Serum was collected 21 d after booster immunization, heat inactivated at 56° C for 30 min,  
286 aliquoted and stored at 4° C. Abs and serum were titrated and specificity was tested, by flow  
287 cytometry on HEK293-FT cells transiently expressing SARS-CoV-2 N (Addgene # 141391), S  
288 (BEI # NR-52310) or S<sup>st</sup>.

## 289 **Immunofluorescence**

290 For confocal microscopy imaging, 2.5 x 10<sup>4</sup> cells were seeded on 12 mm glass coverslips in 24-  
291 well plates in indicated medium with gentamycin (25 µg/ml) overnight. Cell were infected with  
292 SARS-CoV-2 at an MOI of 1 PFU/cell for 1 h at 37° C. Virus was aspirated, and cells then  
293 incubated in cell growth media. After 24 h, the cells were washed with DPBS (Gibco # 14190-  
294 144) containing 5% goat serum (Jackson ImmunoResearch Labs. 005-000-121). Primary and  
295 secondary Abs were incubated with live cells at 4° C for 30 min. Cells were then washed twice  
296 with DPBS/5% goat serum and fixed in 4% PFA for 30 min at room temp. After fixation,  
297 coverslips were washed in DPBS and deionized iH<sub>2</sub>O, and mounted with Dapi Fluoromount G<sup>TM</sup>  
298 mounting medium (VWR # 102092-102). Images were acquired with a Leica STELLARIS 8  
299 confocal microscope platform equipped with ultraviolet and white light lasers, using a 63x oil  
300 immersion objective (Leica Microsystems # 11513859), with a 1x zoom resolution of 512 x 512  
301 pixels. Maximum intensity projections (MIPs) were processed from z-stacks (at least 15 0.3 µm z-  
302 steps per image); and for background correction (Gaussian filter) and color processing, using  
303 Imaris (Bitplane). Background levels of signal for each cell type were set based on mock-infected  
304 stained conditions. Animations (gifs) were generated with Photoshop 2022 (Adobe). Tile scans  
305 were taken of representative infected areas and individual fields (tiles) were merged into one  
306 image. Mock-infected coverslips were processed in parallel with infected counterparts, and SARS-  
307 CoV-2-infected coverslips were also incubated with all secondary Abs only as controls, and  
308 images were acquired using identical photomultiplier and laser settings.

## 309 **Flow cytometry**

310 For cell surface protein expression analyses, 1 x 10<sup>5</sup> cells were seeded on 24-well plates and mock  
311 or SARS-CoV-2-infected at an MOI of 1 pfu for 1 h at 37° C, followed by aspirating the virus  
312 inoculum and adding medium containing 2% FBS. After the indicated hpi, the cells were washed

313 with DPBS, trypsinized with TrypLE™ Express Enzyme (Thermo Fisher # 12604039) or 0.25%  
314 Trypsin-EDTA (Thermo Fisher # 25200056) for 5 min at 37° C, transferred to a 96 well plate and  
315 washed with HBSS (Lonza # 10-527F) with 0.1% BSA. Cells were stained live with Alexa Fluor-  
316 conjugated Abs (or primary and secondary Abs), and LIVE/DEAD™ Fixable Violet Dead Cell  
317 Stain Kit (Thermo Fisher # L34964) in DPBS, for 25 min at 4° C. After Ab staining, cells were  
318 twice washed with HBSS 0.1% BSA and then fixed in 4% PFA for 30 min at room temp. PFA was  
319 aspirate and cells were resuspended in HBSS 0.1% BSA for analysis. To control for possible  
320 removal of cell surface antigens by trypsinization, in parallel infected cells after 24 h were washed  
321 with DPBS and directly stained in the 24 well plate prior to trypsinization. This resulted in similar  
322 levels of cell surface viral protein detection between trypsinized-stained and vice versa conditions.

323 For cell surface protein binding assays using recombinant proteins, indicated cells were  
324 trypsinized, washed with DPBS, and  $1 \times 10^5$  cells transferred to 96-well plates. Indicated amounts  
325 of recombinant GFP-His (Thermo Fisher # A42613) or SARS-CoV-2 N-His (Sino Biological #  
326 40588-V08B, Acro Biosystems # NUN-C5227, Ray Biotech # 230-30164) were resuspended in  
327 100  $\mu$ l of DPBS, and cells were incubated for 15 min at 37° C and orbital shaking of 150 rpm.  
328 Cells were washed twice and stained as described above for subsequent flow cytometry analysis.  
329 For electric charge neutralization assays, after incubation with recombinant proteins and twice  
330 washed, cells were incubated with 10  $\mu$ g/ml of polybrene (MilliporeSigma # TR-1003-G) in DPBS  
331 for 15 min at 37° C and orbital shaking of 150 rpm. Then, cells were washed twice and stained as  
332 described above for subsequent analysis.

333 For heparinase assays,  $1 \times 10^5$  single cells in 96-well plates were treated with Bacteroides  
334 heparinase I (4.8 units), II (1.6 units) and III (0.28 units) (NEB # P0735S, # P0736S, # P0737S) in  
335 DPBS for 1 h at 30° C. Cells were washed twice, incubated with recombinant proteins, and stained  
336 as described above for subsequent analysis.

337 For transient surface protein expression,  $2 \times 10^5$  cells were seeded on 12-well plates and transiently  
338 transfected with 2  $\mu$ g of plasmids encoding SARS-CoV-2 N (Addgene # 141391) or eGFP  
339 (Addgene # 141395) with TransIT-LT1. At indicated time post transfection, cells were processed  
340 as described above for cell surface protein binding assays.

341 For every assay and condition, at least 30,000 cells were analyzed on an BD FACSCelesta™ Cell  
342 Analyzer (BD Biosciences) with a high throughput system unit, and quadrants in double staining  
343 plots were set based on mock-infected condition for each cell type. Data were analyzed with  
344 FlowJo (Tree Star) and plotted with Prism v9.1.1 software (GraphPad).

#### 345 **Cell co-culture assays**

346 For infectable and non-infectable cell co-culture assays,  $9 \times 10^5$  cells of each indicated SARS-  
347 CoV-2-non-infectable cell type were stained with CellTrace™ Violet (Thermo Fisher # C34557),  
348 following manufacturer's instructions, and seeded in 6-well plates. Then,  $1 \times 10^5$  CHO-K1\_hACE2  
349 cells (SARS-CoV-2-infectable) were homogeneously mixed and co-seeded with indicated non-  
350 infectable cell type, being co-cultured overnight. Co-cultured cells were inoculated with SARS-  
351 CoV-2 at an MOI of 1 for 1 h at 37° C, followed by removal of the virus inoculum and replacement  
352 of the medium containing 2% FBS. After 24 h, cells were washed with DPBS and directly stained  
353 live on their 6 wells with Alexa Fluor®-conjugated Abs and LIVE/DEAD™ Fixable Violet Dead  
354 Cell Stain Kit, in DPBS for 25 min at 4° C. After staining, cells were washed twice with HBSS  
355 0.1% BSA, trypsinized with TrypLE™ Express Enzyme for 5 min at 37° C, transferred to 96 wells,

356 washed with HBSS 0.1% BSA and fixed in 4% PFA for 30 min at room temp. PFA was aspirated  
357 and cells were resuspended in HBSS 0.1% BSA for flow cytometry analysis.

358 For transfected and non-transfected cell co-culture assays,  $2 \times 10^5$  cells were seeded on 6-well  
359 plates and transiently transfected with 2  $\mu\text{g}$  of plasmids encoding SARS-CoV-2 N or eGFP with  
360 TransIT-LT1. After 24 h,  $9 \times 10^5$  non-transfected cells were stained with CellTrace™ Violet and  
361 co-seeded with their transfected homologs, being co-cultured for 24 h. Then, cells were washed  
362 with DPBS and directly stained live on their 6 wells with Alexa Fluor®-conjugated Abs and  
363 LIVE/DEAD™ Fixable Violet Dead Cell Stain Kit, in DPBS for 25 min at 4° C. Cells were washed  
364 twice with HBSS 0.1% BSA, trypsinized with TrypLE™ Express Enzyme for 5 min at 37° C,  
365 transferred to 96 wells, washed twice with HBSS 0.1% BSA and resuspended in HBSS 0.1% BSA  
366 for flow cytometry analysis.

367 For every assay and condition, at least 100,000 cells were analyzed on an BD FACSCelesta™ Cell  
368 Analyzer with a high throughput system unit, and data were analyzed with FlowJo and plotted  
369 with GraphPad Prism software.

### 370 **Cytokines and GAGs**

371 Recombinant human cytokines used in this study (CCL1, CCL2, CCL3, CCL3L1, CCL4,  
372 CCL4L1, CCL5, CCL7, CCL8, CCL11, CCL13, CCL14, CCL15, CCL16, CCL17, CCL18,  
373 CCL19, CCL20, CCL21, CCL22, CCL23, CCL24, CCL25, CCL26, CCL27, CCL28, CXCL1,  
374 CXCL2, CXCL3, CXCL4, CXCL5, CXCL6, CXCL7, CXCL8, CXCL9, CXCL10, CXCL11,  
375 CXCL12 $\alpha$ , CXCL12 $\beta$ , CXCL13, CXCL14, CXCL16, XCL1, CX3CL1, IL-1 $\alpha$ , IL-1 $\beta$ , IL-6, IL-  
376 6R $\alpha$ , IL-10, IL-12p70, IL-13, IL-17a, IL-18BP-Fc, IL-23, IL-27, IL-35, TNF- $\alpha$ , TNF- $\beta$ , IFN- $\beta$ ,  
377 IFN- $\gamma$ , IFN- $\lambda$ 1, IFN- $\omega$ ) from PeproTech, and (IFN- $\alpha$ 2 and IL-18) from Sino Biological, were  
378 reconstituted in DPBS 0.1% BSA at 10  $\mu\text{M}$ , aliquoted and stored at -80° C. Heparin (# 2106),  
379 heparan sulfate from bovine kidney (# H7640), chondroitin sulphate A (# C9819) and chondroitin  
380 sulphate B (# C3788) were obtained from MilliporeSigma. Heparan sulfate from porcine mucosa  
381 (# AMS.GAG-HS01) and keratan sulfate (# AMS.CSR-NAKPS2-SHC-1) were purchased from  
382 ASMBIO. We assumed an average molecular weight of 30 kDa for heparan sulfate from porcine  
383 mucosa and 15 kDa for heparin <sup>36</sup>.

### 384 **BLI assays**

385 High throughput binding assays were performed on an Octet Red384 (ForteBio) instrument at 30°  
386 C with shaking at 1,000 rpm. Streptavidin (SA) biosensors (Sartorius # 18-5019) were hydrated  
387 for 15 min in kinetics buffer (DPBS, 1% BSA, 0.05% Tween-20). SARS-CoV-2 structural proteins  
388 and accessory factors (2X-StrepTag tagged) in lysis buffer from commercial sources or crude  
389 lysates of transfected cells (see details below) were loaded into SA biosensors up to 0.5-5 nm of  
390 binding response for 300-600 s, prior to baseline equilibration for 180 s in kinetics buffer.  
391 Association of each analyte in kinetics buffer at indicated concentration was carried out for 300 s,  
392 followed by dissociation for 300 s or longer. Standard binding and kinetic assays between SARS-  
393 CoV-2 N and GAGs or chemokines were performed as described above for binding assays.  
394 Negative signal of N binding to GAGs, expected given the large size of heparin molecules, was  
395 flipped prior further analysis <sup>37</sup>. The data were baseline subtracted prior to fitting performed using  
396 the homogeneous (1:1) and heterogeneous binding models (2:1, mass transport, 1:2) within the  
397 ForteBio Data Analysis HT software v12.0.1.55. Mean  $K_D$ ,  $k_{on}$ ,  $k_{off}$  values were determined with  
398 a global fit applied to all data. The performance of each binding model fitting to the data was  
399 assessed based on the lowest sum of the squared deviations or measure of error between the

400 experimental data and the fitted line ( $\chi^2$ ), and the highest correlation between fit and experimental  
401 data ( $R^2$ ).

402 The experiments were repeated with at least three independently produced batches of recombinant  
403 protein in crude lysates, obtained from  $30 \times 10^6$  HEK293-FT cells transfected with 30  $\mu\text{g}$  of  
404 plasmids encoding SARS-CoV-2 structural proteins and accessory factors with TransIT-LT1.  
405 SARS-CoV-2 St containing 2X-StrepTag at the C-terminal region was commercially synthesized  
406 as mentioned above (GenScript Biotech). SARS-CoV-2 N, M, E, ORF3a, ORF3b, ORF6, ORF7a,  
407 ORF7b, ORF8, ORF9b, ORF9c and ORF10 plasmids without signal peptide for secretion,  
408 described in <sup>38</sup>, were acquired from Addgene ([www.addgene.org/Nevan\\_Krogan](http://www.addgene.org/Nevan_Krogan)). After 24 h,  
409 transfected cells were selected with 10  $\mu\text{g}/\text{ml}$  of puromycin (Invivogen # ant-pr-1). After 48 h,  
410 transfected cells were trypsinized, washed with DPBS and lysated for 30 min at 4° C in 1 ml of  
411 lysis buffer (50 mM Tris-HCl pH 7.4, 150 mM NaCl, 5 mM KCl, 5 mM MgCl<sub>2</sub>, 1% NP-40 and  
412 1x protease inhibitors (Roche # 4693159001)), followed by centrifugation at 1000 x g at 4° C.  
413 Clarified supernatants (crude lysates) were collected, aliquoted, stored at -20° C and characterized  
414 by immunoblotting using mouse anti-2xStrep tag (Qiagen #34850, 1:1,000), and secondary goat  
415 anti-mouse IgG IRDye® 800CW (LI-COR # 926-32210, 1:10,000). rN was additionally  
416 characterized by immunoblotting using IRDye® 680RD Streptavidin (LI-COR # 926-68079), and  
417 human anti-SARS-CoV-2 N mAb (N18) followed by IRDye® 680RD Goat anti-Human IgG  
418 Secondary Ab (LI-COR # 926-68078).

419 For GAGs competition assays of chemokine binding, selected chemokines (100 nM) were  
420 incubated in kinetics buffer alone or with indicated concentrations of soluble heparan sulfate from  
421 bovine kidney, chondroitin sulfate A and chondroitin sulfate B for 10 min at room temp. The  
422 mixture was used to measure the association of N (in nM of binding response), as described above  
423 for the BLS binding assays. The value in nm of binding response of each chemokine binding  
424 without GAGs was considered 100%.

#### 425 **Chemotaxis assays**

426 Recombinant human CXCL12 $\beta$  (3 nM), alone or in combination with purified recombinant  
427 proteins were placed in the lower chamber of a 96-well ChemoTx System plate (Neuro Probe #  
428 101-3 and # 101-5) in RPMI 1640 1% FBS. As internal controls within each assay, medium or  
429 recombinant protein alone were used. PBMCs, MonoMac-1 and MOLT-4 cells ( $1.25 \times 10^5$ ) were  
430 placed on the upper compartment and separated from the lower chamber by a 3 or 5  $\mu\text{m}$  pore size  
431 filter. The cells were incubated at 37° C for 3 h in a humidified incubator with 5% CO<sub>2</sub>. The  
432 migrated cells in the lower chamber were stained with 5  $\mu\text{l}$  of CellTiter 96 AQueous One Solution  
433 Cell Proliferation Assay (Promega # G3580) for 2 h at 37° C with 5% CO<sub>2</sub>, measuring absorbance  
434 at 490 nm using a Synergy H1 plate reader (Bio-Tek).

435 The following recombinant proteins were used: SARS-CoV-2 S1-His (Sino Biological # 40591-  
436 V08B1), SARS-CoV-2 N-His (Sino Biological # 40588-V08B), SARS-CoV-2 N-His (Acro  
437 Biosystems # NUN-C5227), SARS-CoV-2 N-His (Ray Biotech # 230-30164), SARS-CoV-1 N-  
438 His (Acro Biosystems # NUN-S5229) and MERS-CoV N-His (Acro Biosystems # NUN-M52H5).  
439 SARS-CoV-2 N-His from Sino Biological (# 40588-V08B) was used in all assays unless indicated.

#### 440 **ADCC reporter assay**

441 For each indicated cell type,  $1 \times 10^4$  cells were seeded on 96-well flat white tissue culture-treated  
442 plates (Thermo Fisher # 136101), cultured overnight, and infected with SARS-CoV-2 at an MOI

443 of 1 (target cells). At 24 hpi, infected target cells were washed with DPBS and the medium was  
444 replaced with 50  $\mu$ l of RPMI 1640 with 4% low IgG serum (Promega # G711A) containing 5 x  
445  $10^4$  Jurkat effector cells (Promega # G701A) and serial dilutions of indicated human mAbs. After  
446 overnight incubation at 37° C with 5% CO<sub>2</sub>, 50  $\mu$ l of Bright-Glo™ Luciferase Assay lysis/substrate  
447 buffer (Promega # E2620) were added and luminescence was measured after 10 min using a  
448 POLARstar Omega plate reader (BMG LABTECH) within the luciferase Glow assay template and  
449 the following parameters: gain 3600; measurement interval time 0.1 s; and maximum counts 2 x  
450  $10^6$ . Measurements were performed in triplicate and relative luciferase units (RLU) were plotted  
451 and analyzed with GraphPad Prism software. Data fitting with GraphPad Prism was performed  
452 with the non-linear regression dose-response-stimulation model.

### 453 **Statistical analysis**

454 Statistical analyses were performed using GraphPad Prism software. When indicated, *p* values  
455 were calculated using Student's two-tailed unpaired *t* test (at 99% confidence interval) and *p* <  
456 0.01 was considered statistically significant. On the other hand, One-way ANOVA and Dunnett's  
457 Multiple comparison test (at 95% confidence interval) was used to compare all conditions against  
458 untreated or mock-infected cells (as indicated for each case), considering *p* < 0.05 as statistically  
459 significant.

460

461

462

463

464

465

466

467

468

469

470

471

472

473

474

475

476

477

478

479

## 480 REFERENCES

- 481 1 Long, Q. X. *et al.* Antibody responses to SARS-CoV-2 in patients with COVID-19. *Nat. Med.* **26**,  
482 845-848, doi:10.1038/s41591-020-0897-1 (2020).
- 483 2 Sariol, A. & Perlman, S. Lessons for COVID-19 Immunity from Other Coronavirus Infections.  
484 *Immunity* **53**, 248-263, doi:10.1016/j.immuni.2020.07.005 (2020).
- 485 3 Yewdell, J. W., Frank, E. & Gerhard, W. Expression of influenza A virus internal antigens on the  
486 surface of infected P815 cells. *J Immunol.* **126**, 1814-1819 (1981).
- 487 4 Yewdell, J. W. *et al.* Recognition of cloned vesicular stomatitis virus internal and external gene  
488 products by cytotoxic T lymphocytes. *J Exp Med.* **163**, 1529-1538, doi:10.1084/jem.163.6.1529  
489 (1986).
- 490 5 Staerz, U. D., Yewdell, J. W. & Bevan, M. J. Hybrid antibody-mediated lysis of virus-infected  
491 cells. *Eur J Immunol.* **17**, 571-574 (1987).
- 492 6 Lamere, M. W. *et al.* Contributions of Antinucleoprotein IgG to Heterosubtypic Immunity against  
493 Influenza Virus. *J Immunol.* **186**, 4331-4339, doi:10.4049/jimmunol.1003057 (2011).
- 494 7 Marie, J. C. *et al.* Cell surface delivery of the measles virus nucleoprotein: a viral strategy to induce  
495 immunosuppression. *J Virol.* **78**, 11952-11961, doi:10.1128/jvi.78.21.11952-11961.2004 (2004).
- 496 8 Céspedes, P. F. *et al.* Surface expression of the hRSV nucleoprotein impairs immunological  
497 synapse formation with T cells. *Proc Natl Acad Sci U S A.* **111**, E3214-3223,  
498 doi:10.1073/pnas.1400760111 (2014).
- 499 9 Straub, T. *et al.* Nucleoprotein-specific nonneutralizing antibodies speed up LCMV elimination  
500 independently of complement and FcγR. *Eur J Immunol.* **43**, 2338-2348,  
501 doi:https://doi.org/10.1002/eji.201343565 (2013).
- 502 10 Ikuta, K. *et al.* Expression of human immunodeficiency virus type 1 (HIV-1) gag antigens on the  
503 surface of a cell line persistently infected with HIV-1 that highly expresses HIV-1 antigens.  
504 *Virology* **170**, 408-417, doi:10.1016/0042-6822(89)90431-5 (1989).
- 505 11 Buchrieser, J. *et al.* Syncytia formation by SARS-CoV-2-infected cells. *EMBO J.* **39**, e106267,  
506 doi:10.15252/embj.2020106267 (2020).
- 507 12 Van Phan, H. *et al.* Fixed single-cell RNA sequencing for understanding virus infection and host  
508 response. *bioRxiv.* doi:10.1101/2020.09.17.302232 (2021).
- 509 13 Boson, B. *et al.* The SARS-CoV-2 envelope and membrane proteins modulate maturation and  
510 retention of the spike protein, allowing assembly of virus-like particles. *J Biol Chem.* **296**, 100111,  
511 doi:10.1074/jbc.RA120.016175 (2021).
- 512 14 Dinesh, D. C. *et al.* Structural basis of RNA recognition by the SARS-CoV-2 nucleocapsid  
513 phosphoprotein. *PLoS Pathog.* **16**, e1009100, doi:10.1371/journal.ppat.1009100 (2020).
- 514 15 Zinzula, L. *et al.* High-resolution structure and biophysical characterization of the nucleocapsid  
515 phosphoprotein dimerization domain from the Covid-19 severe acute respiratory syndrome  
516 coronavirus 2. *Biochem Biophys Res Commun.* **538**, 54-62, doi:10.1016/j.bbrc.2020.09.131 (2021).
- 517 16 Capila, I. & Linhardt, R. J. Heparin-protein interactions. *Angew Chem Int Ed Engl.* **41**, 391-412,  
518 doi:10.1002/1521-3773(20020201)41:3<390::aid-anie390>3.0.co;2-b (2002).
- 519 17 Hossler, P., Khattak, S. F. & Li, Z. J. Optimal and consistent protein glycosylation in mammalian  
520 cell culture. *Glycobiology* **19**, 936-949, doi:10.1093/glycob/cwp079 (2009).
- 521 18 Nakanaga, K., Yamanouchi, K. & Fujiwara, K. Protective effect of monoclonal antibodies on lethal  
522 mouse hepatitis virus infection in mice. *J Virol.* **59**, 168-171, doi:10.1128/jvi.59.1.168-171.1986  
523 (1986).
- 524 19 Lecomte, J. *et al.* Protection from mouse hepatitis virus type 3-induced acute disease by an anti-  
525 nucleoprotein monoclonal antibody. Brief report. *Arch Virol.* **97**, 123-130,  
526 doi:10.1007/bf01310740 (1987).
- 527 20 Supekar, N. T. *et al.* Variable post-translational modifications of SARS-CoV-2 nucleocapsid  
528 protein. *Glycobiology* **9**, 1080-1092, doi:10.1093/glycob/cwab044 (2021).

- 529 21 Rabouille, C. Pathways of Unconventional Protein Secretion. *Trends Cell Biol.* **27**, 230-240,  
530 doi:10.1016/j.tcb.2016.11.007 (2017).
- 531 22 Katsinelos, T. *et al.* Unconventional Secretion Mediates the Trans-cellular Spreading of Tau. *Cell*  
532 *Rep.* **23**, 2039-2055, doi:10.1016/j.celrep.2018.04.056 (2018).
- 533 23 Gonzalez-Motos, V., Kropp, K. A. & Viejo-Borbolla, A. Chemokine binding proteins: An  
534 immunomodulatory strategy going viral. *Cytokine Growth Factor Rev.* **30**, 71-80,  
535 doi:10.1016/j.cytogfr.2016.02.007 (2016).
- 536 24 Hernaez, B. & Alcamí, A. Virus-encoded cytokine and chemokine decoy receptors. *Curr Opin*  
537 *Immunol.* **66**, 50-56, doi:10.1016/j.coi.2020.04.008 (2020).
- 538 25 Gaebler, C. *et al.* Evolution of antibody immunity to SARS-CoV-2. *Nature* **591**, 639-644,  
539 doi:10.1038/s41586-021-03207-w (2021).
- 540 26 Grootemaat, A. E. *et al.* Lipid and nucleocapsid N-protein accumulation in COVID-19 patient lung  
541 and infected cells. *bioRxiv*. doi:10.1101/2021.06.24.449252 (2021).
- 542 27 Liu, S. J. *et al.* Immunological characterizations of the nucleocapsid protein based SARS vaccine  
543 candidates. *Vaccine* **24**, 3100-3108, doi:10.1016/j.vaccine.2006.01.058 (2006).
- 544 28 Dangi, T., Class, J., Palacio, N., Richner, J. M. & Penaloza MacMaster, P. Combining spike- and  
545 nucleocapsid-based vaccines improves distal control of SARS-CoV-2. *Cell Rep.* **36**, 109664,  
546 doi:10.1016/j.celrep.2021.109664 (2021).
- 547 29 Joag, V. *et al.* Cutting Edge: Mouse SARS-CoV-2 Epitope Reveals Infection and Vaccine-Elicited  
548 CD8 T Cell Responses. *J Immunol.* **206**, 931-935, doi:10.4049/jimmunol.2001400 (2021).
- 549 30 Matchett, W. E. *et al.* Cutting Edge: Nucleocapsid Vaccine Elicits Spike-Independent SARS-CoV-  
550 2 Protective Immunity. *J Immunol.* **207**, 376-379, doi:10.4049/jimmunol.2100421 (2021).
- 551 31 Sagara, I. *et al.* SARS-CoV-2 seroassay optimization and performance in a population with high  
552 background reactivity in Mali. *medRxiv*. doi:10.1101/2021.03.08.21252784 (2021).
- 553 32 Kowarz, E., Löscher, D. & Marschalek, R. Optimized Sleeping Beauty transposons rapidly  
554 generate stable transgenic cell lines. *Biotechnol J.* **10**, 647-653, doi:10.1002/biot.201400821  
555 (2015).
- 556 33 Zhao, A. *et al.* Isolation and identification of an scFv antibody against nucleocapsid protein of  
557 SARS-CoV. *Microbes Infect.* **9**, 1026-1033, doi:10.1016/j.micinf.2007.04.008 (2007).
- 558 34 Wu, Y. *et al.* A noncompeting pair of human neutralizing antibodies block COVID-19 virus binding  
559 to its receptor ACE2. *Science* **368**, 1274-1278, doi:10.1126/science.abc2241 (2020).
- 560 35 Wrapp, D. *et al.* Cryo-EM structure of the 2019-nCoV spike in the prefusion conformation. *Science*  
561 **367**, 1260-1263, doi:10.1126/science.abb2507 (2020).
- 562 36 Schulman, S. & Levi, M. *Chapter 32: Antithrombotic Therapy in Williams Hematology, 10th*  
563 *Edition.*
- 564 37 Cameron, C. *et al.* Octet® Potency Assay: Development, Qualification and Validation Strategies.  
565 doi:https://www.sartorius.com/download/789382/octet-potency-assay-development-validation-  
566 strategies-applic-2--data.pdf (2021).
- 567 38 Gordon, D. E. *et al.* A SARS-CoV-2 protein interaction map reveals targets for drug repurposing.  
568 *Nature* **583**, 459-468, doi:10.1038/s41586-020-2286-9 (2020).

569

570

571

572

573

574

575

576 **ACKNOWLEDGMENTS**

577 We thank James S. Gibbs for outstanding technical assistance. We are grateful to the NIAID  
578 SARS-CoV-2 Virology Core BSL3 Laboratory staff for their training, help, and support. This work  
579 was supported by the Division of Intramural Research of the National Institute of Allergy and  
580 Infectious Diseases.

581

582 **AUTHOR CONTRIBUTIONS**

583 A.D.L.M. conceived, designed, and performed experiments, analyzed data, interpreted results, and  
584 wrote the manuscript.

585 I.K. produced in-house antibodies, and helped to design and analyze ADCC assays.

586 J.H. generated cell lines expressing hACE2.

587 J.W.Y. conceived experiments and wrote the manuscript.

588

589 **COMPETING INTERESTS**

590 The authors declare no competing interests.

591

592 **Supplementary Information is available for this paper.**

593

594 **MATERIALS & CORRESPONDENCE**

595 Correspondence and material requests should be addressed to J.W.Y.

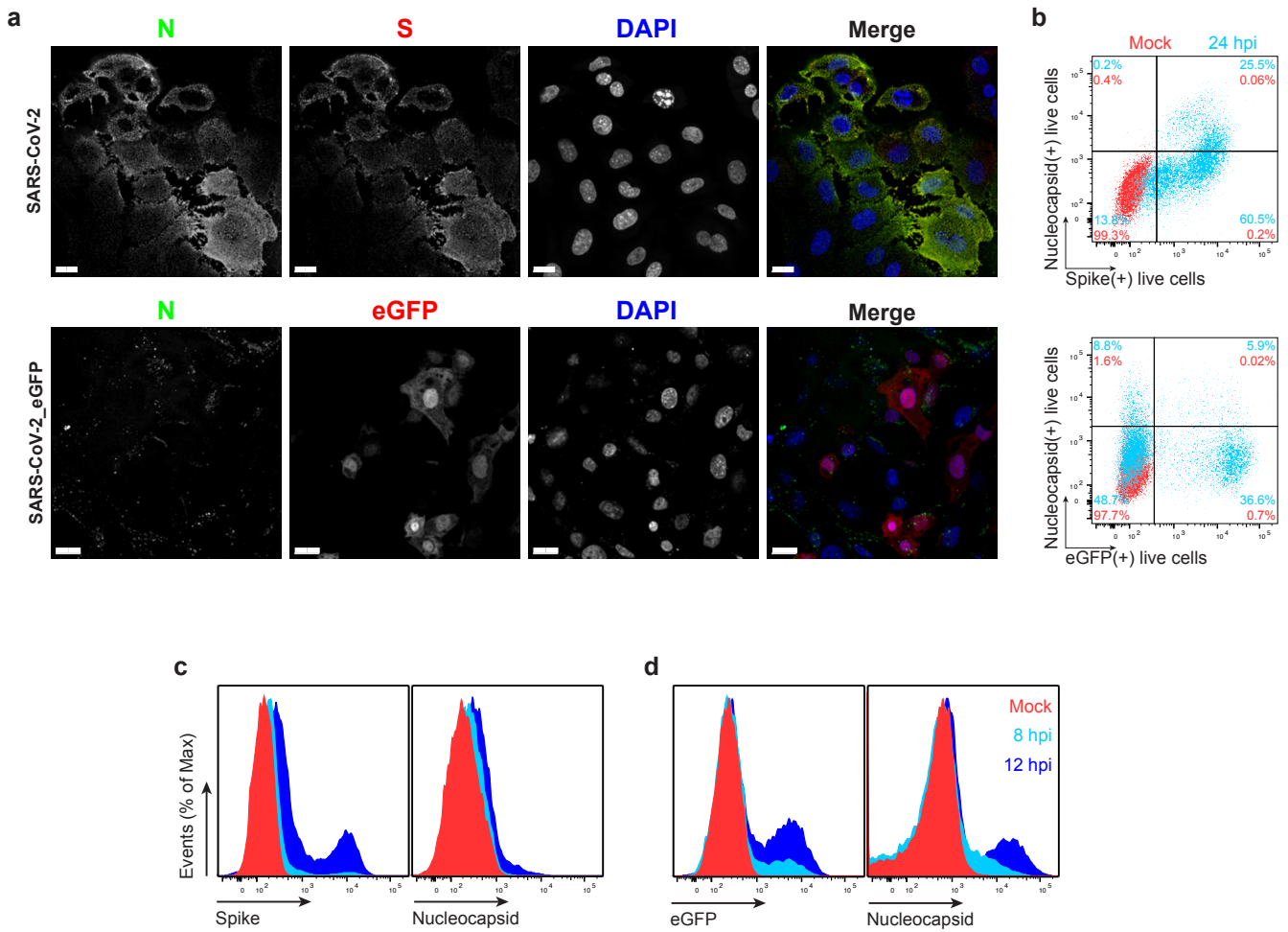


**Fig. 1: SARS-CoV-2 N is expressed on the surface of live cells early during infection.** **a**, Maximum intensity projections (MIP) of laser confocal microscopy z-stack images of infected Vero cells with wild-type SARS-CoV-2 (top panels) or SARS-CoV-2\_eGFP, stained live at 24 hpi (MOI = 1). Scale bar = 20  $\mu$ m. Images are representative of at least three independent experiments with similar results. **b**, Flow cytometry analyses of Vero cells inoculated with wild-type (top) or eGFP expressing (bottom) SARS-CoV-2 (MOI = 1), stained live at 24 hpi against SARS-CoV-2 S and N proteins. Representative dot plots of flow cytometry analyses showing double staining of surface S and N, and eGFP proteins, indicating the percentage of the gated cell population for each quadrant of the double staining. Data are representative of at least three independent experiments, each performed with triplicate samples. **c**, **d**, Time course of surface S, N, and eGFP proteins expression in live infected Vero cells with wild-type (**c**) and eGFP reporter (**d**) SARS-CoV-2 at 8 and 12 hpi (MOI = 1). Representative histogram overlays of surface S, N, and intracellular eGFP proteins of flow cytometry analyses. Data are representative of one experiment out of at least two independent experiments performed in triplicate.

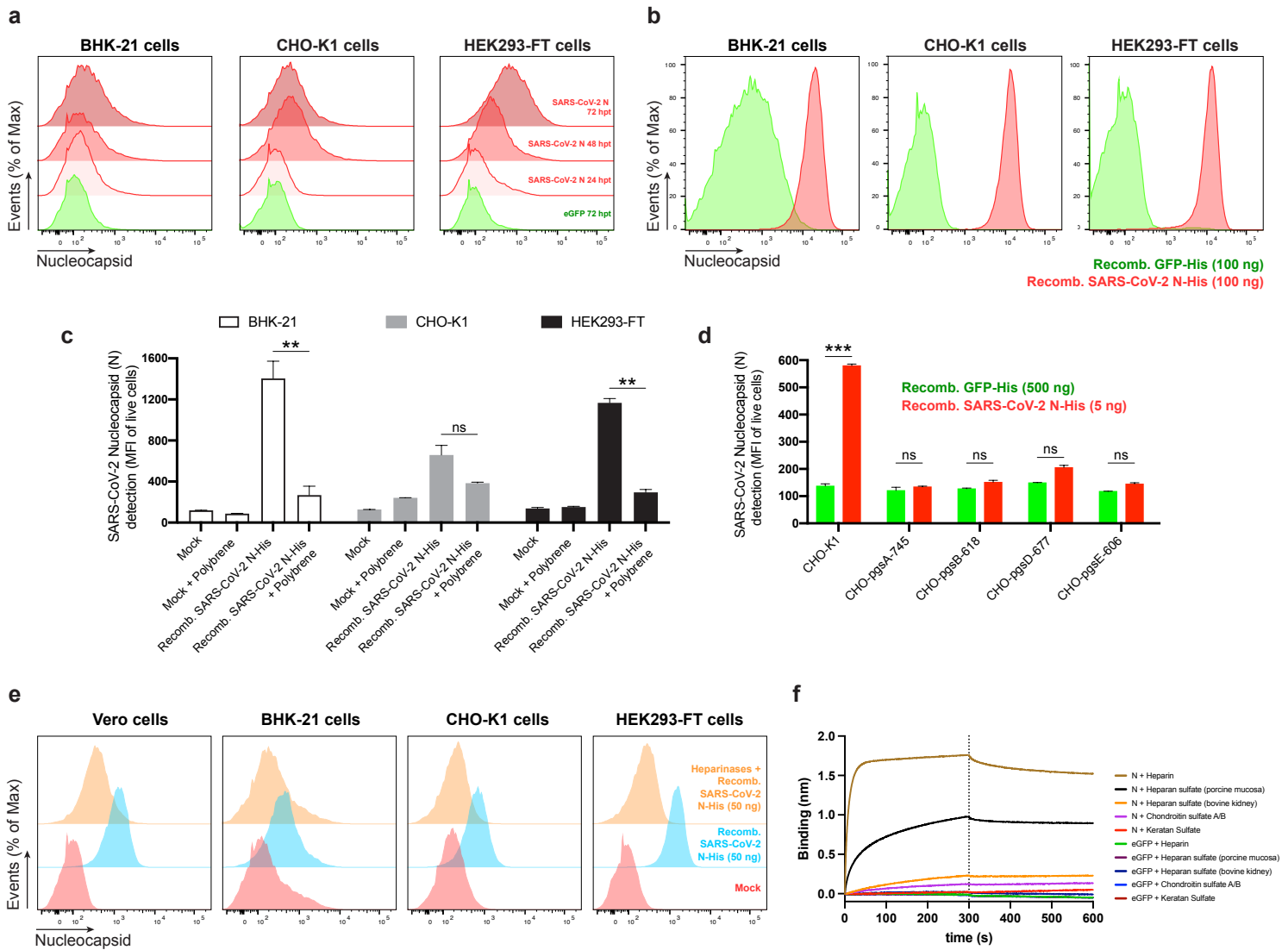


**Fig. 2: SARS-CoV-2 N cell surface binding is independent of other viral genes and is specifically mediated by heparan sulfate/heparin.** **a**, Histogram semi-overlays of kinetics (24-72 h) of surface N protein expression in BHK-21, CHO-K1 and HEK293-FT cells transiently transfected with a plasmid encoding eGFP or N protein, detected with Abs by flow cytometry. **b**, Histogram overlays of analyses of exogenous rN binding to BHK-21, CHO-K1 and HEK293-FT cells, incubated with recombinant eGFP or N protein for 15 min, washed twice, stained live with Abs, and analyzed by flow cytometry. **c**, Electric charge neutralization assays with a cationic polymer (polybrene). BHK-21, CHO-K1 and HEK293-FT cells were incubated with 50 ng of rN protein for 15 min, washed twice, incubated with 10  $\mu$ g/ml of polybrene, washed twice again, stained live with Abs, and analyzed by flow. **d**, Different GAG-deficient CHO cells were incubated with recombinant eGFP or N protein for 15 min, washed twice, stained live with Abs, and analyzed by flow cytometry. **e**, Heparinase treatment completely abrogates the cell ability to bind and retain N protein. Flow cytometry histogram semi-overlays of BHK-21, CHO-K1 and HEK293-FT cells treated with heparinases for 1 h, washed twice, incubated with 50 ng of rN protein for 15 min, washed twice again, stained live with Abs, and analyzed. **f**, BLI sensorgrams from binding assays of sulfated GAGs to immobilized N or eGFP proteins. Streptavidin-coated biosensors were loaded with equivalent amounts of N or eGFP, measuring their ability to bind each GAG. Sensorgrams show association and dissociation phases, where the vertical dotted line indicates the end of the association step. In **c**, **d**, the mean fluorescent intensity (MFI) of detected surface N protein from live cells is plotted, showing mean  $\pm$  SEM ( $n = 2$ ). Student's two-tailed unpaired *t*-test was used to compare N-incubated cells vs. N-incubated and polybrene treated cells (**c**), and to compare GFP- vs. N-incubated cells (**d**): *ns* (statistically nonsignificant)  $p > 0.01$ ,  $** p < 0.01$ ,  $*** p < 0.001$ . The analyses were repeated with different protein preparations, and one representative assay out of at least three independent assays performed in duplicate is shown.

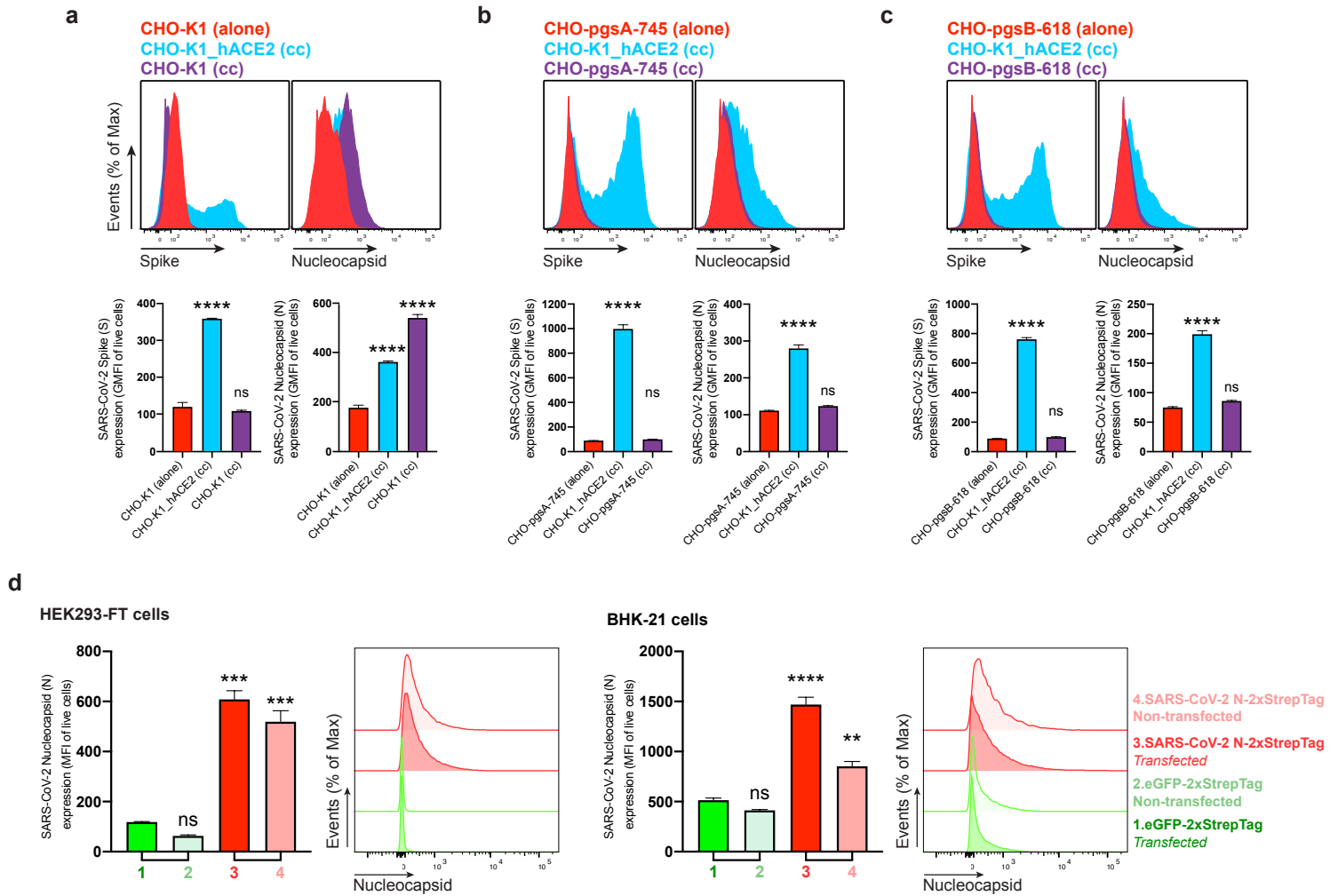


**Fig. 3: SARS-CoV-2 N protein is transferred to the cell surface of neighboring uninfected cells.** Flow cytometry analyses of N transfer assays between donor and recipient co-cultured cells. **a-c**, N transfer assays between infectable and non-infectable co-cultured cells. CHO-K1 (**a**), GAG-deficient CHO-pgsA-745 (**b**) and CHO-pgsB-618 (**c**) cells (non-infectable), alone or co-cultured (cc) with CHO-K1\_hACE2 cells (infectable), were inoculated with SARS-CoV-2 (MOI = 1) and stained live with Abs at 24 hpi against surface SARS-CoV-2 S and N proteins. Non-infectable cells were stained with CellTrace™ Violet prior co-culture with infectable cells (**Supplementary Fig. 1**). For dot plots showing double staining of surface S and N with percentages of the gated cell population for each quadrant see **Supplementary Fig. 1c-e**. **d**, N transfer assays between transfected and non-transfected co-cultured cells. HEK293-FT and BHK-21 cells were transiently transfected with a plasmid encoding eGFP or N protein. After 24 h, non-transfected HEK293-FT or BHK-21 cells were stained with CellTrace™ Violet prior to be added and co-cultured with their transfected counterparts. Cells were stained live after 24 h with Abs and analyzed. For each assay, the following is shown: histogram overlays and semi-overlays of surface N and S proteins, as well as the GMFI or MFI geometric MFI (GMFI) of live cells expressing S and N proteins is plotted, showing mean  $\pm$  SEM ( $n = 3$ ). One representative experiment of at least three independent experiments performed in triplicate is shown. One-way ANOVA and Dunnett's Multiple comparison test were used to compare all conditions against non-infectable cells cultured alone within each assay, or against eGFP-transfected cells: ns (nonsignificant)  $p > 0.05$ , \*\*  $p < 0.01$ , \*\*\*  $p < 0.001$ , \*\*\*\*  $p < 0.0001$ .

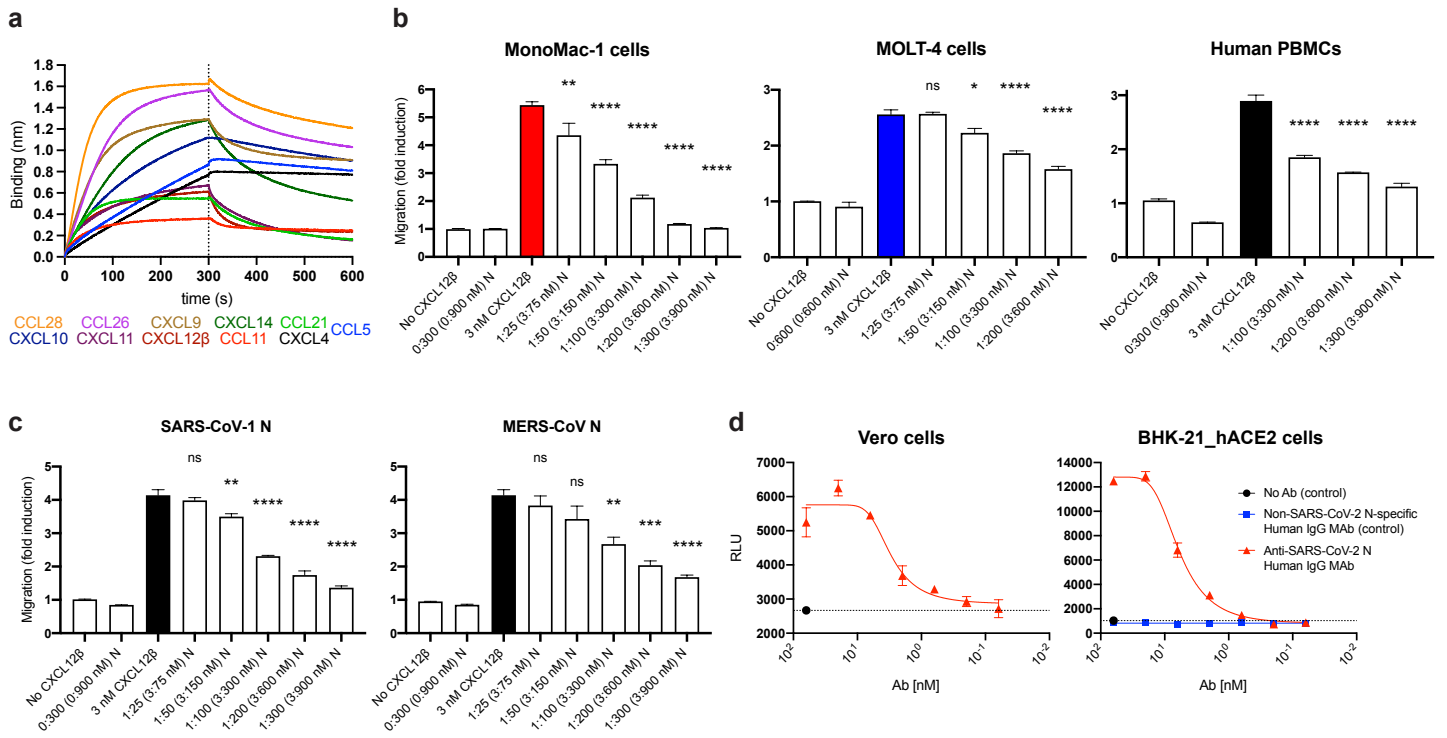
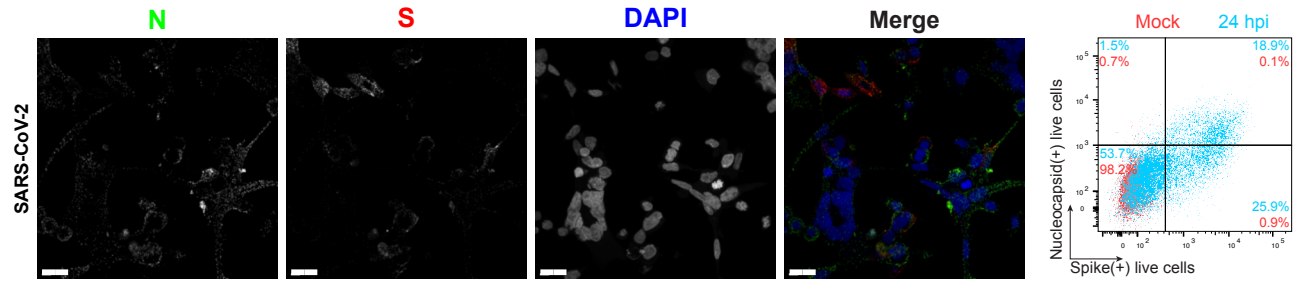
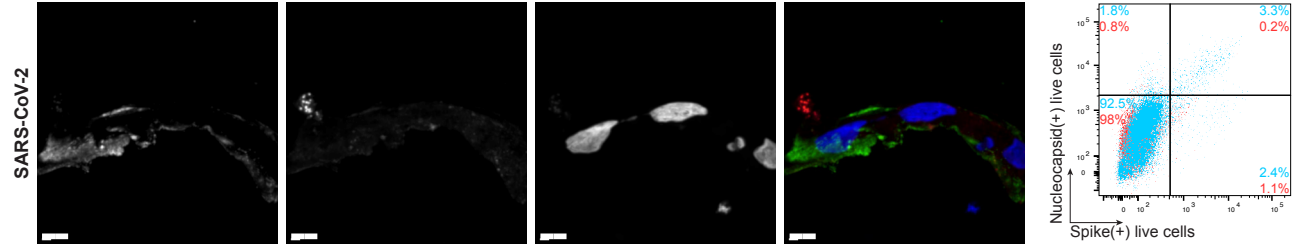


**Fig. 4: SARS-CoV-2 N protein modulates innate and adaptive immunity.** **a, b,** N binds chemokines through the GAG-binding domain of chemokines and inhibits in vitro chemokine-mediated leukocyte migration. **a,** BLI sensorgrams of binding assays showing association and dissociation phases of the interaction between N protein and 11 positively bound chemokines at a concentration of 100 nM out of 64 human cytokines tested. The dotted line indicates the end of the association step. The analyses were repeated with different purified rN protein preparations. One representative assay of three independent assays is shown. **b,** SARS-CoV-2 N blocks CXCL12 $\beta$  chemotaxis of MonoMac-1 cells, MOLT-4 cells and human PBMCs. **c,** SARS-CoV-1 N and MERS-CoV N block CXCL12 $\beta$  chemotaxis of MonoMac-1 cells. CXCL12 $\beta$  was incubated alone or in the presence of the indicated viral protein in the lower chamber of transwell migration devices. Migrated cells from the top chamber were detected in the lower chamber at the end of the experiment. The induction of migration shows means  $\pm$  SEM ( $n = 3$ ) from one representative assay performed in triplicate out of at least three independent assays. One-way ANOVA and Dunnett's Multiple comparison test were used to compare all conditions (except no chemokine and viral protein alone conditions) against migration induced by chemokine alone (colored bar): *ns* (nonsignificant)  $p > 0.05$ , \*  $p < 0.05$ , \*\*  $p < 0.01$ , \*\*\*  $p < 0.001$ , \*\*\*\*  $p < 0.0001$ . **d,** N protein is a target for Ab-based immunity. ADCC reporter bioassays were performed on SARS-CoV-2-infected Vero and BHK-21\_hACE2 target cells (24 hpi, MOI =1) using decreasing concentrations of a human mAb against the N protein and Jurkat effector reporter cells. After overnight incubation, luciferase expression to gauge cell activation was measured. Data show mean  $\pm$  SEM ( $n = 3$ ) of one representative assay out of three independent experiments performed in triplicate. Dashed lines show background signal detected in the absence of Ab.

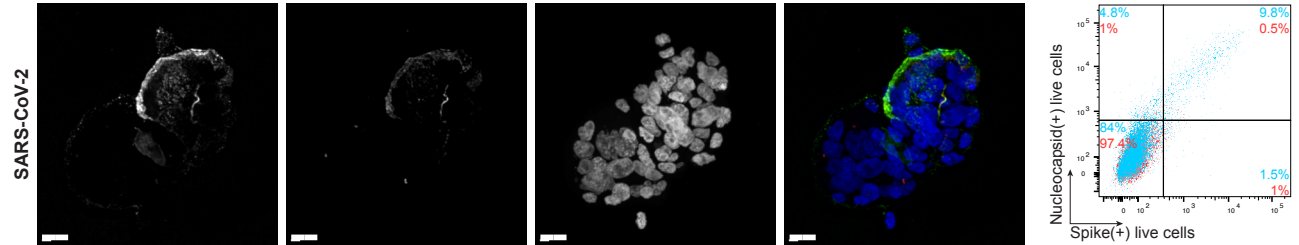
BHK-21 hACE2 cells



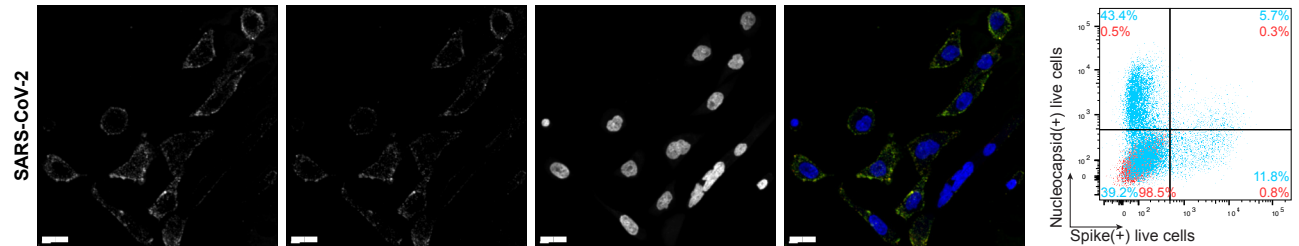
Caco-2 cells



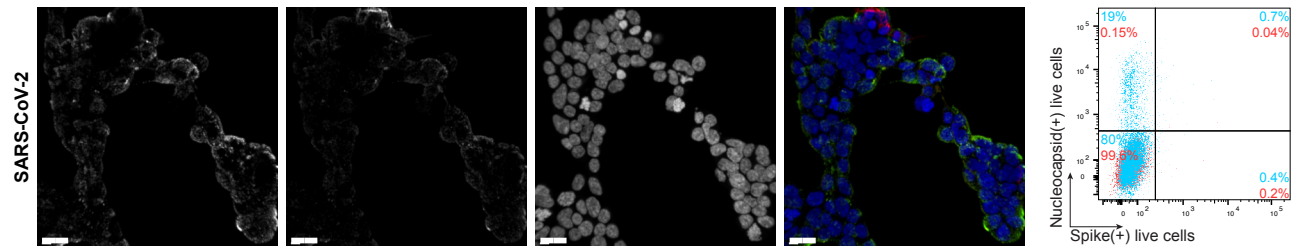
Calu-3 cells



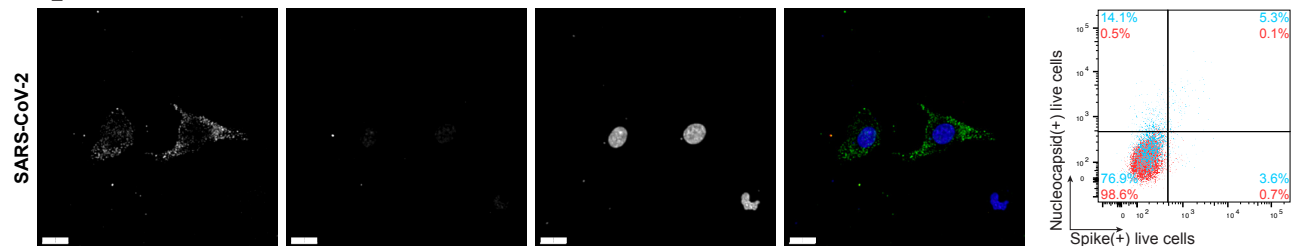
CHO-K1\_hACE2 cells



HEK293-FT\_hACE2 cells

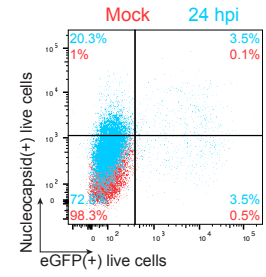
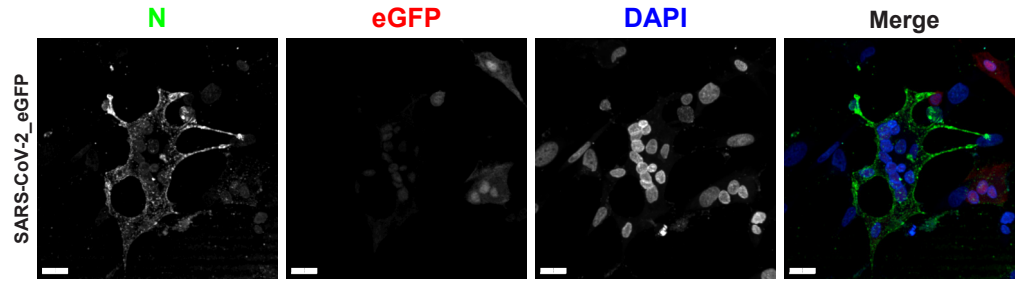


A549\_hACE2 cells

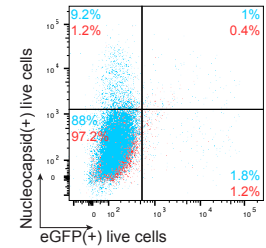
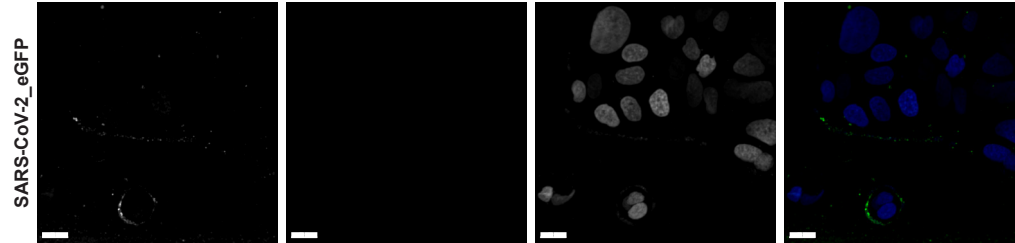


**Extended Data Fig. 1: SARS-CoV-2 N protein is expressed on the cell surface of diverse infected cell types.** Maximum intensity projections (MIP) of laser confocal microscopy z-stack images and histogram overlays of flow cytometry analyses of live wild-type SARS-CoV-2-infected BHK-21\_hACE2, Caco-2, Calu-3, CHO-K1\_hACE2, HEK293-FT\_hACE2 and A549\_hACE2 cells stained live with Abs at 24 hpi (MOI = 1). Scale bars = 20  $\mu$ m. Images are representative of three independent experiments with similar results. Representative plots of flow cytometry analyses show double staining of surface S and N, indicating the percentage of the gated cell population for each quadrant of the double staining. Data are representative of one experiment out of at least three independent experiments performed in triplicate.

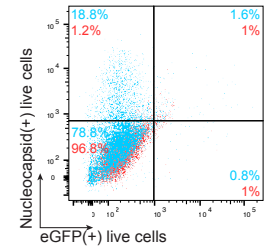
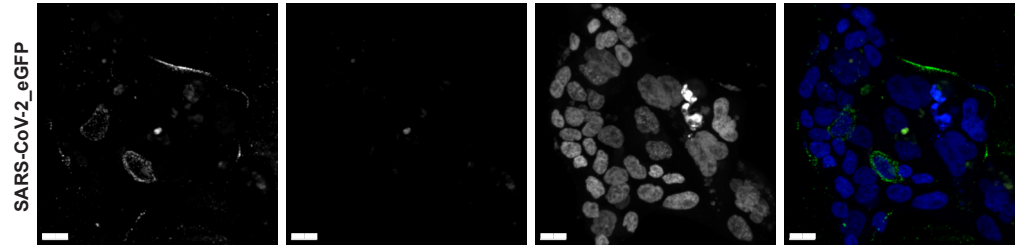
BHK-21 hACE2 cells



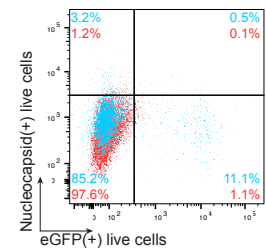
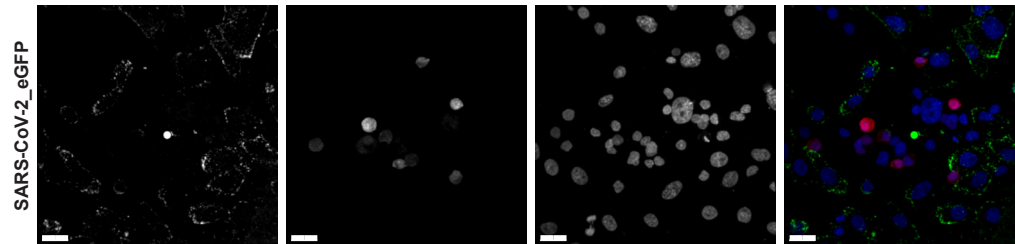
Caco-2 cells



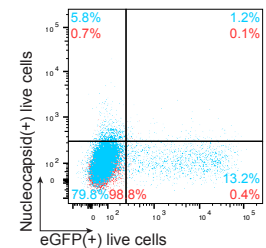
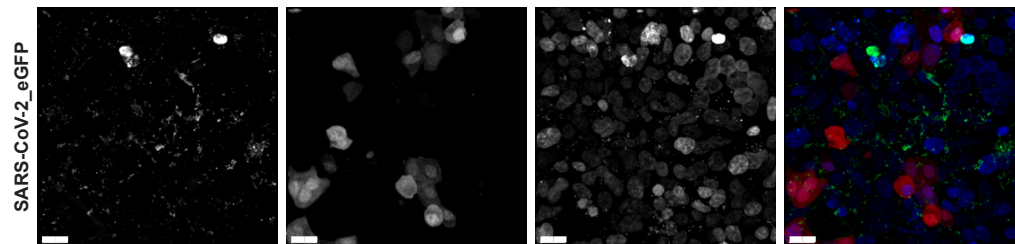
Calu-3 cells



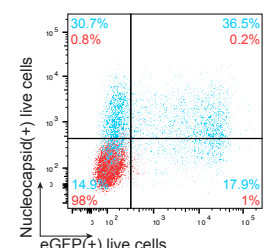
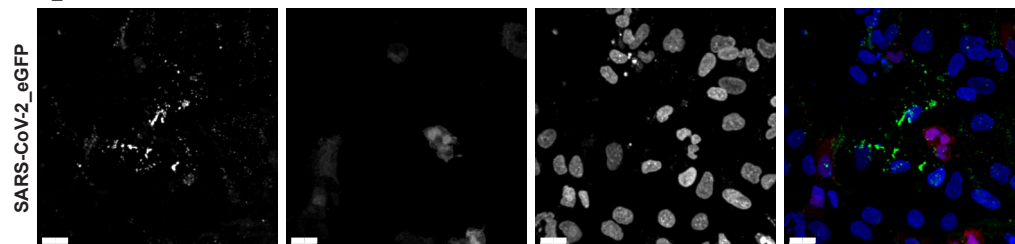
CHO-K1\_hACE2 cells



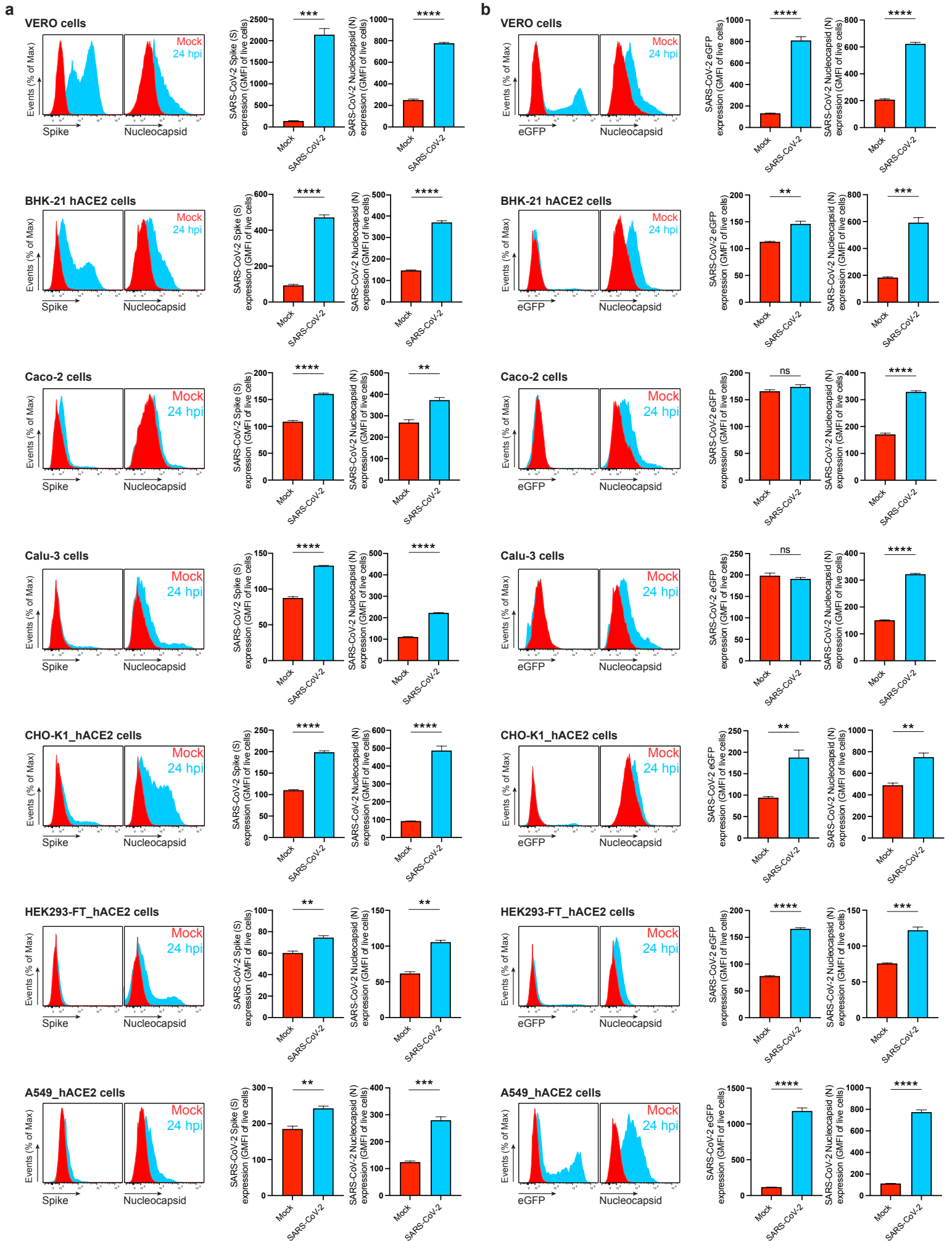
HEK293-FT\_hACE2 cells



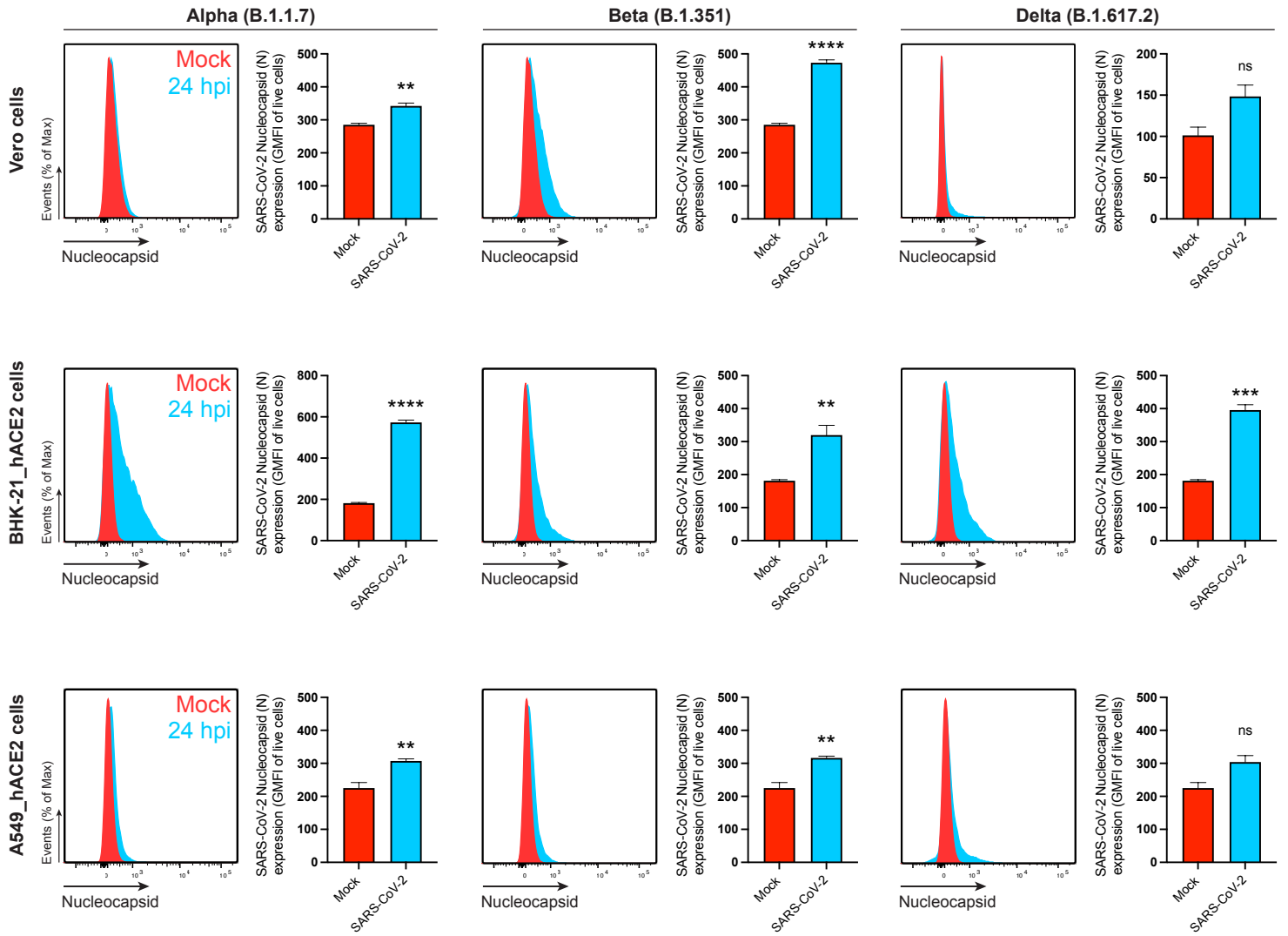
A549\_hACE2 cells



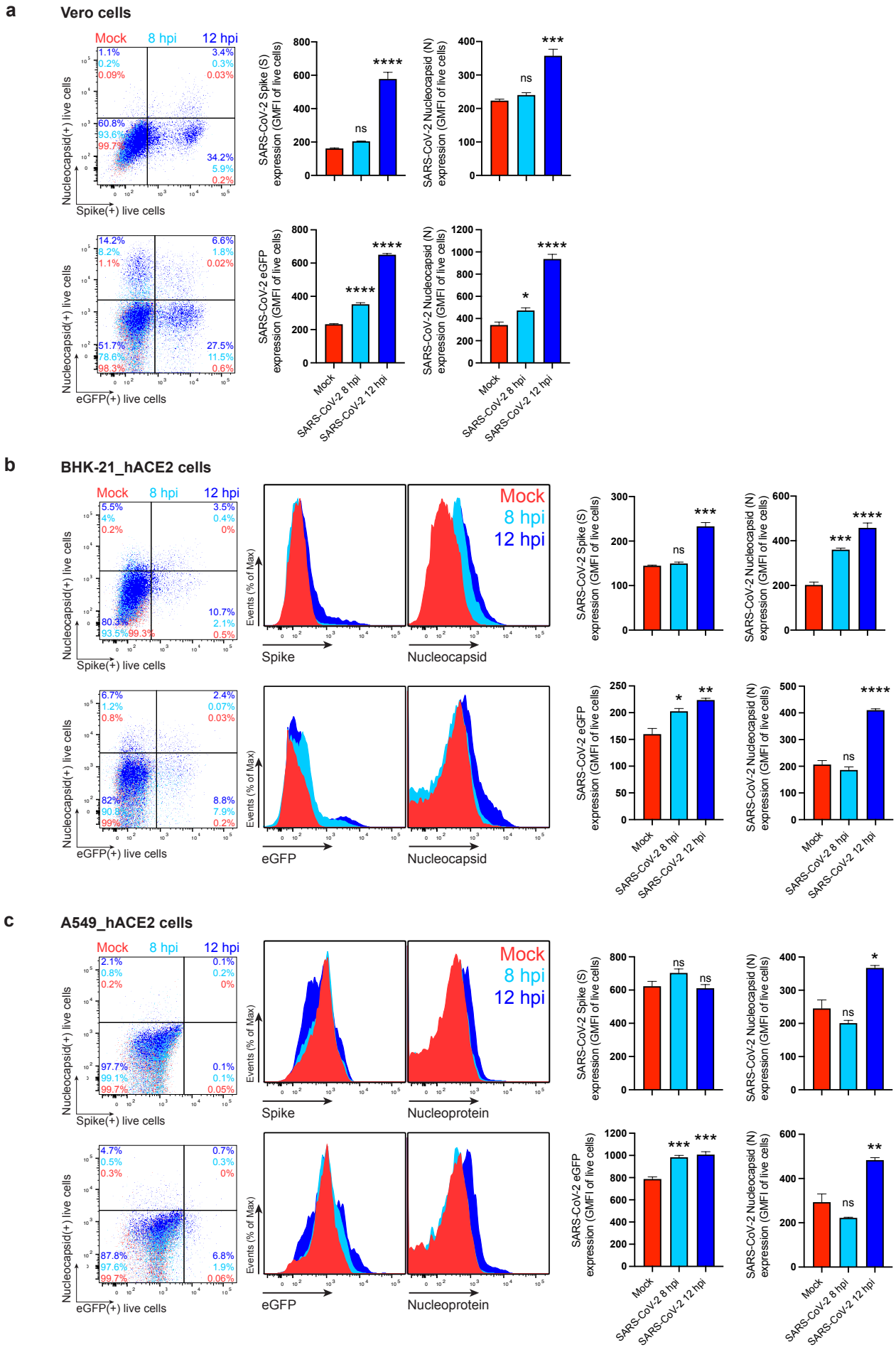
**Extended Data Fig. 2: SARS-CoV-2 N protein is a robust marker of cell-surface infection across cell types.** MIP of laser confocal microscopy z-stack images and histogram overlays of flow cytometry analyses of live eGFP expressing SARS-CoV-2-infected BHK-21\_hACE2, Caco-2, Calu-3, CHO-K1\_hACE2, HEK293-FT\_hACE2 and A549\_hACE2 cells stained live with MAb against N at 24 hpi (MOI = 1). Scale bars = 20  $\mu$ m. Images are representative of two independent experiments with similar results. Representative plots of flow cytometry analyses show double staining of eGFP and surface N, indicating the percentage of the gated cell population for each quadrant of the double staining. Data are representative of one experiment out of at least three independent experiments performed in triplicate.



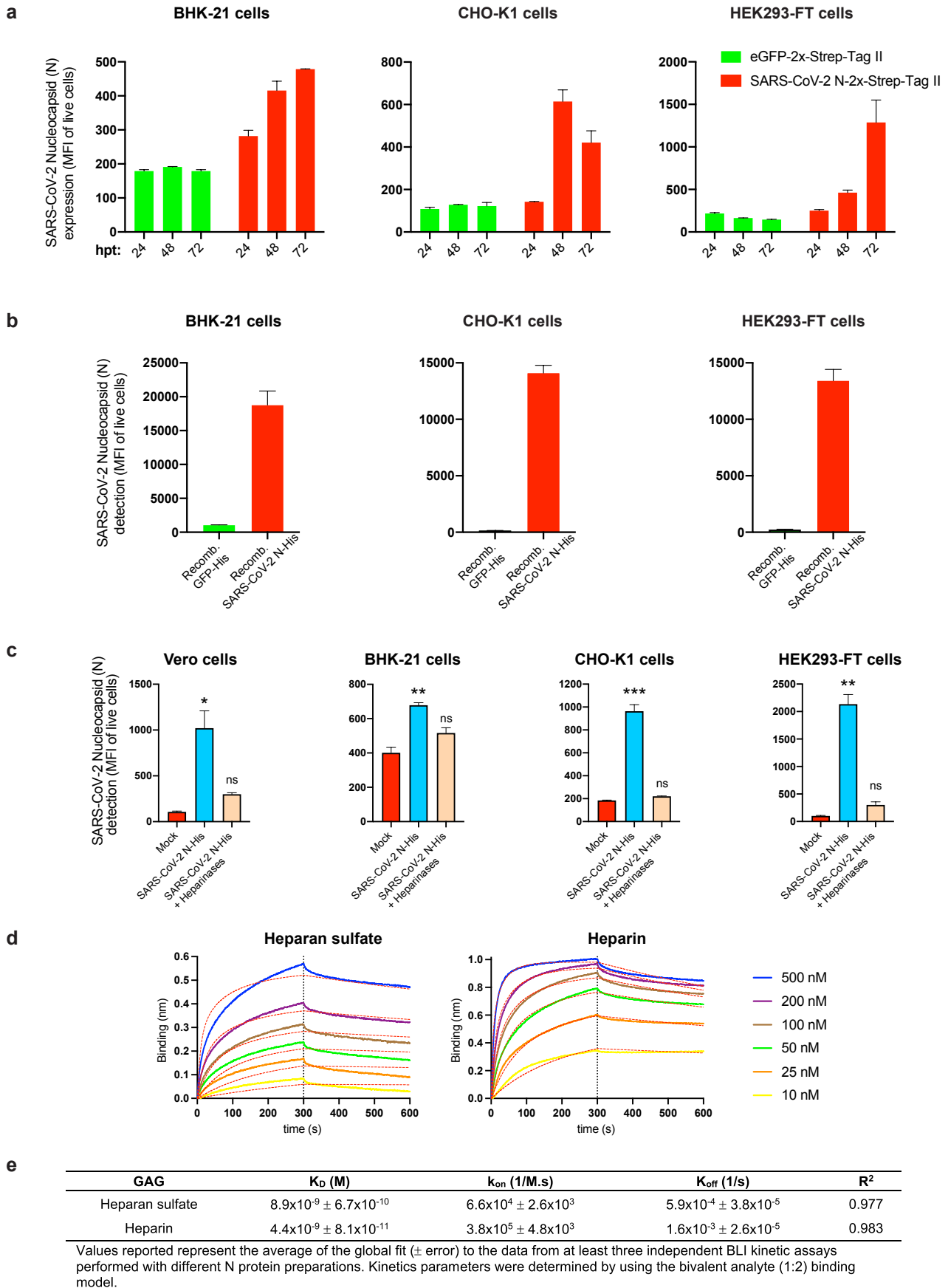
**Extended Data Fig. 3: SARS-CoV-2 N is significantly detected on the cell surface of all live infected cell types tested in this study.** Flow cytometry analyses of Vero, BHK-21\_hACE2, Caco-2, Calu-3, CHO-K1\_hACE2, HEK293-FT\_hACE2 and A549\_hACE2 cells inoculated with wild-type (a) or eGFP reported (b) SARS-CoV-2 (MOI = 1), and stained live with Abs at 24 hpi against SARS-CoV-2 S and N proteins. For each cell type and infection, the following is shown: histogram overlays of surface S and N, and intracellular eGFP, as well as the GMFI is plotted showing mean  $\pm$  SEM (n = 3). Histogram overlays correspond to Fig. 1b (Vero cells), while those shown in (a) to Extended Data Fig. 1 and those in (b) to Extended Data Fig. 2. Data are representative of one experiment out of at least three independent experiments performed in triplicate. ns (nonsignificant)  $p > 0.01$ , \*\*  $p < 0.01$ , \*\*\*  $p < 0.001$ , \*\*\*\*  $p < 0.0001$  by Student's two-tailed unpaired *t*-test.



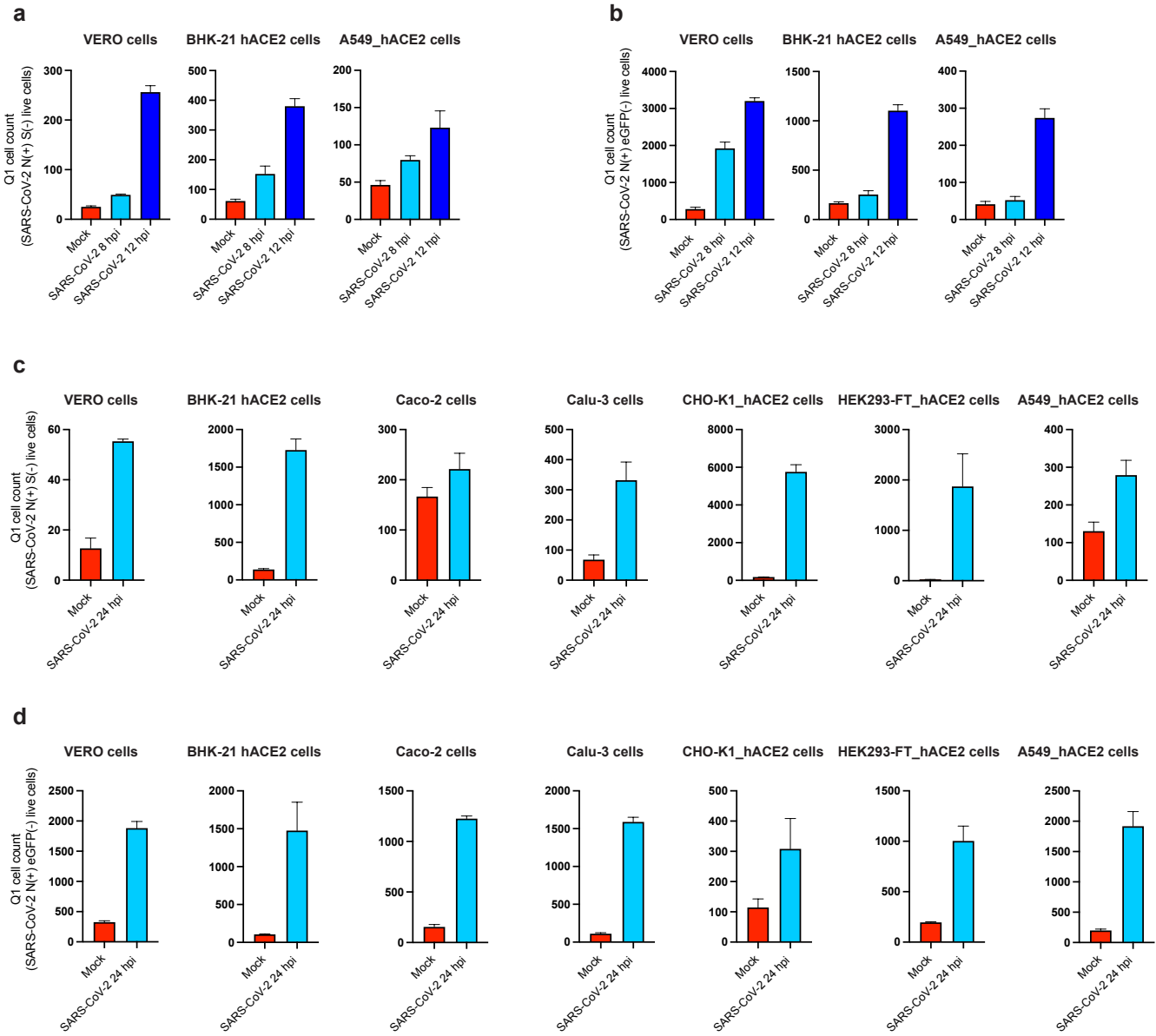
**Extended Data Fig. 4: SARS-CoV-2 N is also detected on the cell surface of live cells infected with the Alpha, Beta and Delta variants.** Flow cytometry analyses of Vero, BHK-21\_hACE2, and A549\_hACE2 cells inoculated with SARS-CoV-2 variants (MOI = 1), and stained live with Abs at 24 hpi against SARS-CoV-2 N. For each cell type and infection, the following is shown: histogram overlays of surface N on live cells, as well as the GMFI is plotted showing mean  $\pm$  SEM (n = 3). Data are representative of one experiment out of at least three independent experiments performed in triplicate. ns (nonsignificant)  $p > 0.01$ , \*\*  $p < 0.01$ , \*\*\*  $p < 0.001$ , \*\*\*\*  $p < 0.0001$  by Student's two-tailed unpaired *t*-test.



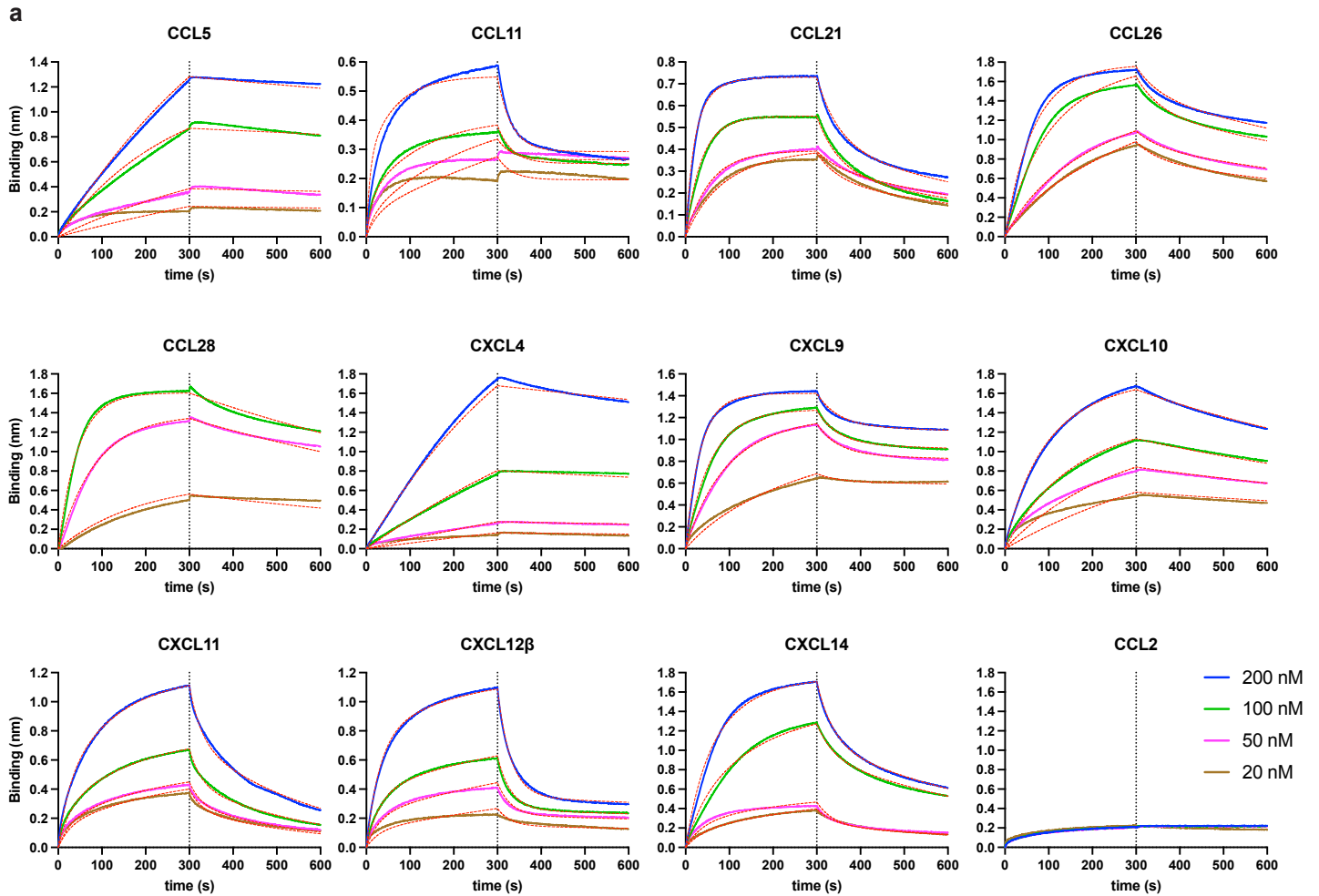
**Extended Data Fig. 5: SARS-CoV-2 N reaches the cell surface as soon as 8 to 12 hpi.** Time course of surface S, N, and eGFP proteins expression in live Vero (a), BHK-21\_hACE2 (b) and A549\_hACE2 cells (c) infected with wild-type and eGFP reporter SARS-CoV-2 at 8 and 12 hpi (MOI = 1). Representative plots of flow cytometry analyses show double staining of surface S, N, and intracellular eGFP, indicating the percentage of the gated cell population for each quadrant. Histogram overlays of surface S and N, and intracellular eGFP are shown, as well as the GMFI is plotted showing mean  $\pm$  SEM ( $n = 3$ ). Histogram overlays from Vero cells analyses are shown in Fig. 1a, b. Data are representative of one experiment out of at least three independent experiments performed in triplicate. One-way ANOVA and Dunnett's Multiple comparison test were used to compare all conditions against mock-infected cells: ns (nonsignificant)  $p > 0.05$ , \*  $p < 0.05$ , \*\*  $p < 0.01$ , \*\*\*  $p < 0.001$ , \*\*\*\*  $p < 0.0001$ .



**Extended Data Fig. 6: Other SARS-CoV-2 genes are not required for N cell surface expression and binding to surface heparan sulfate/heparin.**  
**a**, Flow cytometry analyses of surface N kinetics (24-72 h) expression in BHK-21, CHO-K1 and HEK293-FT cells transiently transfected with a plasmid encoding eGFP or N protein, detected with Abs. **b**, Flow cytometry analyses of exogenous rN binding to BHK-21, CHO-K1 and HEK293-FT cells, incubated with recombinant eGFP or N protein (100 ng) for 15 min, washed twice, stained live with Abs. **c**, Flow cytometry analyses of BHK-21, CHO-K1 and HEK293-FT cells treated with heparinases for 1 h, washed twice, incubated with 50 ng of rN protein for 15 min, washed twice again, stained live with Abs, and analyzed. The MFI of expressed (a) or bound (b, c) surface N protein from live cells is plotted for each case, showing mean  $\pm$  SEM (n = 2). In (c), One-way ANOVA and Dunnett's Multiple comparison test were used to compare all conditions against untreated cells (mock): ns (nonsignificant)  $p > 0.05$ , \*  $p < 0.05$ , \*\*  $p < 0.01$ , \*\*\*  $p < 0.001$ . **d**, BLI sensorgrams of kinetic assays depicting the interaction between immobilized N protein and different concentrations of heparan sulfate and heparin. All curves were analyzed with the ForteBio Data Analysis HT software, where red dashed lines correspond to a global fit of the data using the bivalent analyte model (1:2). **e**, Table showing averaged values from the kinetic analyses of the N protein binding to heparan sulfate and heparin by BLI. All analyses were repeated with different protein preparations, and one representative assay out of at least three independent assays performed in duplicate is shown.



**Extended Data Fig. 7: Additional evidence supporting transfer of N from infected to uninfected cells.** **a – d**, Cells expressing N but no other marker of infection (S or eGFP) increase in a time-dependent manner. Quadrant 1 (Q1) in plots of flow cytometry analyses showing double staining of surface N and S/eGFP identifies a cell subset of cells only expressing N during infection. Bar histograms show mean  $\pm$  SEM ( $n = 3$ ) from Q1 cell counts of cells at 8 and 12 h after infection with wild-type (**a**) or eGFP reporter virus (**b**), as well as at 24 hpi for each cell type analyzed after wild-type (**c**) or eGFP reporter virus (**d**) infection. Data are representative of one experiment out of at least three independent experiments performed in triplicate.

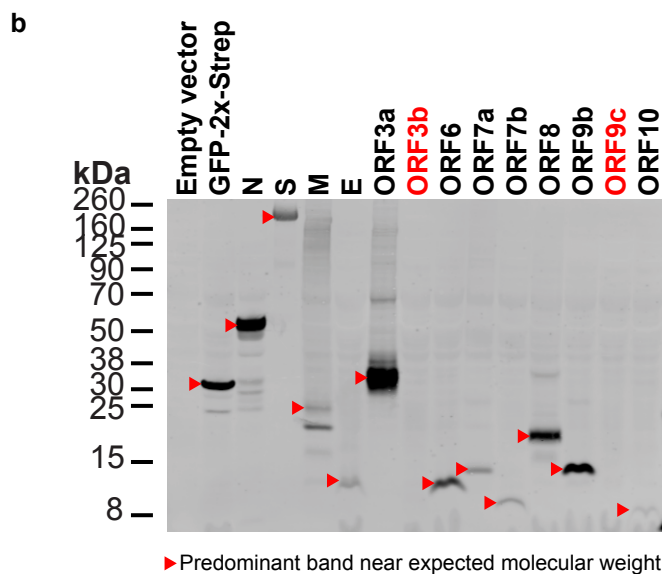
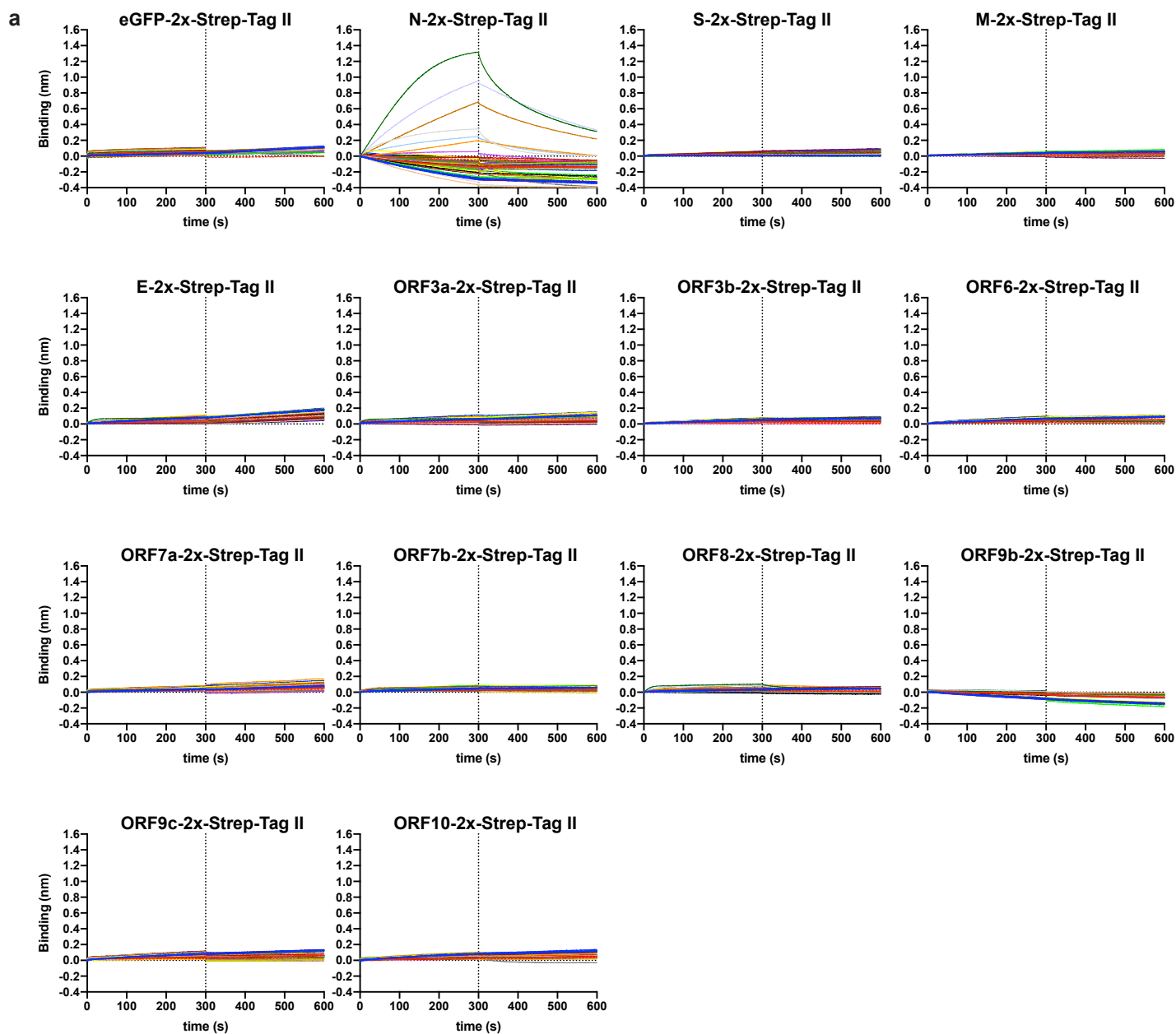


**b**

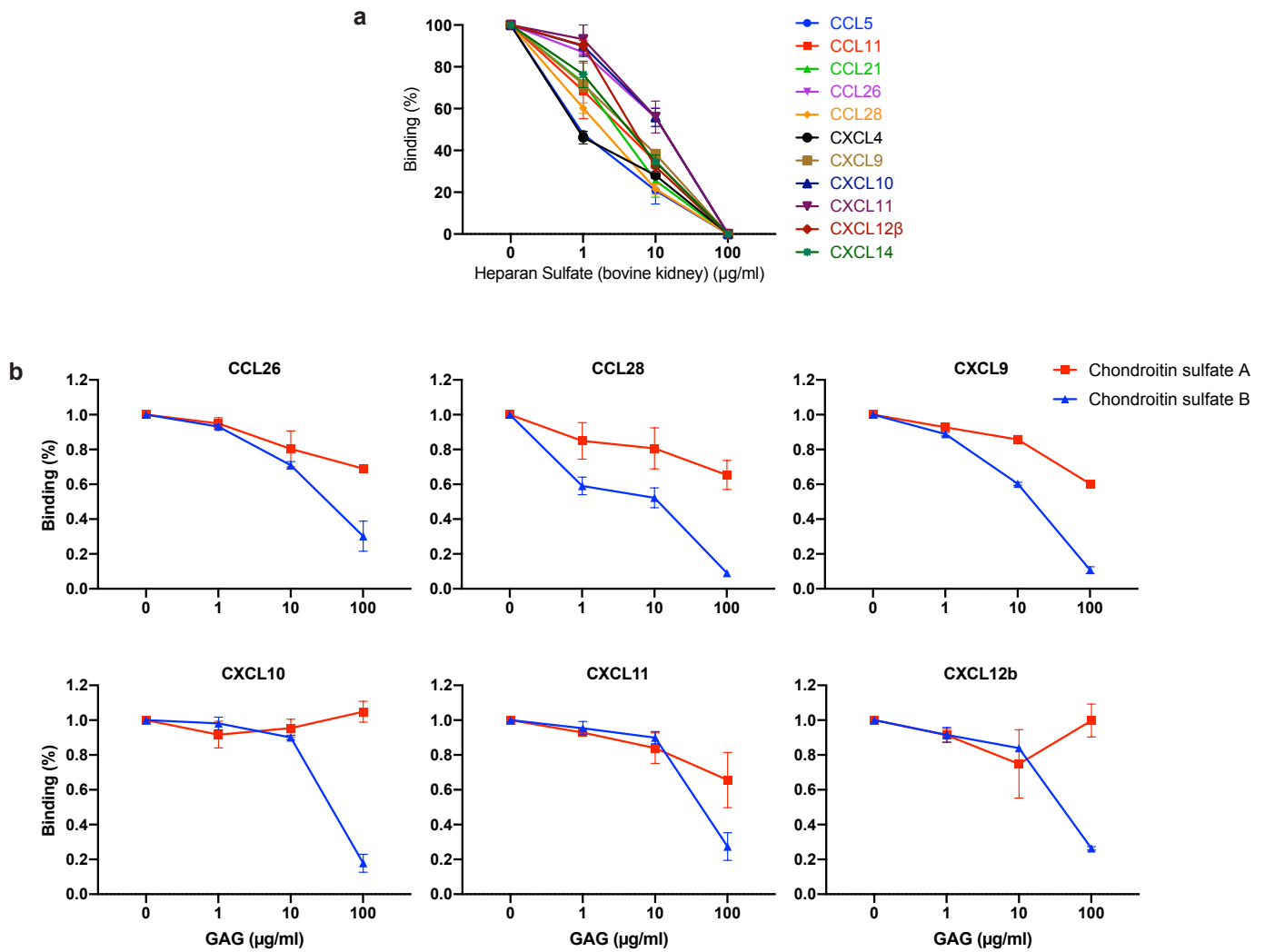
CHK	$K_D$ (M)	$k_{on}$ (1/M.s)	$K_{off}$ (1/s)	$R^2$	Model
CCL5	$1 \times 10^{-8} \pm 1.5 \times 10^{-9}$	$1.9 \times 10^4 \pm 6.5 \times 10^2$	$1.9 \times 10^{-4} \pm 2.7 \times 10^{-5}$	0.977	1:2
CCL11	$7.2 \times 10^{-8} \pm 7.3 \times 10^{-9}$	$1.1 \times 10^5 \pm 4.4 \times 10^3$	$4.5 \times 10^{-3} \pm 1.7 \times 10^{-4}$	0.952	2:1
CCL21	$1.4 \times 10^{-8} \pm 1.9 \times 10^{-10}$	$2.7 \times 10^5 \pm 1.9 \times 10^3$	$1.4 \times 10^{-3} \pm 1.9 \times 10^{-5}$	0.996	2:1
CCL26	$2.6 \times 10^{-8} \pm 6.5 \times 10^{-10}$	$6.3 \times 10^4 \pm 5.7 \times 10^2$	$9.3 \times 10^{-4} \pm 1.1 \times 10^{-5}$	0.997	2:1
CCL28	$2.2 \times 10^{-8} \pm 9.3 \times 10^{-10}$	$1.2 \times 10^5 \pm 8.5 \times 10^2$	$8.7 \times 10^{-4} \pm 1 \times 10^{-5}$	0.996	2:1
CXCL4	$1.7 \times 10^{-7} \pm 1.4 \times 10^{-8}$	$4.2 \times 10^3 \pm 2.6 \times 10^2$	$5.3 \times 10^{-4} \pm 2.1 \times 10^{-5}$	0.997	1:2
CXCL9	$1.2 \times 10^{-8} \pm 1.6 \times 10^{-10}$	$1.2 \times 10^5 \pm 5.4 \times 10^2$	$8.5 \times 10^{-4} \pm 7 \times 10^{-9}$	0.997	2:1
CXCL10	$1 \times 10^{-7} \pm 3.6 \times 10^{-9}$	$1.8 \times 10^4 \pm 3.4 \times 10^2$	$1.6 \times 10^{-3} \pm 4.8 \times 10^{-5}$	0.994	1:2
CXCL11	$1.3 \times 10^{-7} \pm 5.3 \times 10^{-9}$	$4 \times 10^4 \pm 8.1 \times 10^2$	$3.3 \times 10^{-3} \pm 3.6 \times 10^{-5}$	0.985	2:1
CXCL12 $\beta$	$1.7 \times 10^{-7} \pm 1.2 \times 10^{-8}$	$2.2 \times 10^4 \pm 9.6 \times 10^2$	$3.7 \times 10^{-3} \pm 4.9 \times 10^{-5}$	0.991	2:1
CXCL14	$4.5 \times 10^{-8} \pm 5.7 \times 10^{-10}$	$4.4 \times 10^4 \pm 4.5 \times 10^2$	$1.9 \times 10^{-3} \pm 1.6 \times 10^{-5}$	0.996	2:1

Values reported represent the average of the global fit ( $\pm$  error) to the data from at least three independent BLI kinetic assays performed with different N protein preparations. Kinetics parameters were determined by using the heterogeneous ligand (2:1) model or the bivalent analyte (1:2) binding model.

**Extended Data Fig. 8: BLI demonstration that SARS-CoV-2 N protein binds to human chemokines with high affinity.** **a**, BLI sensorgrams of affinity kinetic assays between immobilized SARS-CoV-2 nR protein and positively bound human chemokines identified from BLI HTS binding assays. Sensorgrams show association and dissociation phases. The vertical dotted line indicates the end of the association step. Curves were analyzed with the ForteBio Data Analysis HT software, where red dashed lines correspond to a global fit of the data using the heterogeneous ligand (2:1) or bivalent analyte binding model (1:2). CCL2 is shown as example of negative interaction. All analyses were repeated with different protein preparations, and one representative assay out of at least three independent assays performed in duplicate is shown. **b**, Table showing averaged values from the kinetic analyses of the N protein binding to each chemokine by BLI.



**Extended Data Fig. 9: Among SARS-CoV-2 structural proteins and accessory factors SARS-CoV-2 N protein uniquely binds chemokines. a,** BLI sensorgrams of HTS binding assays between immobilized eGFP, and SARS-CoV-2 structural proteins and accessory factors against 64 human cytokines at 100 nM (see detailed list in Material and Methods). N protein bound CCL5, CCL11, CCL21, CCL26, CCL28, CXCL4, CXCL9, CXCL10, CXCL11, CXCL12 $\beta$  and CXCL14 across different independent assays. Sensorgrams show association and dissociation phases. The dotted line indicates the end of the association step. The analyses were repeated with different protein preparations and one representative assay of two independent HTS is shown. **b,** Immunoblot detection of 2xStrep tag verified expression of predicted protein sizes (red arrowheads), which were loaded into streptavidin-coated biosensors for BLI HTS binding assays. Despite the lack of detection of ORF3b and ORF9c (labeled in red) by immunoblot, the expression of these ORFs was detected after positive loading into streptavidin-coated biosensors by BLI. For gel source data, see **Supplementary Fig. 3.**



**Extended Data Fig. 10: SARS-CoV-2 N protein binds chemokines through the GAG-binding domain of chemokines.** Sulfated GAG competition of chemokine binding to N protein. Chemokines at a concentration of 100 nM, alone or incubated with the indicated increasing concentrations of heparan sulfate from bovine kidney (a) or chondroitin sulfate A/B (b), were used for BLI binding analyses to N protein. The value of each chemokine binding without GAGs was considered 100%. Data represent the mean  $\pm$  SEM of 2-3 independent experiments. Heparan sulfate (from bovine kidney) interaction with N is considered negligible based on results from BLI assays shown in Fig. 2f.

## Supplementary Files

This is a list of supplementary files associated with this preprint. Click to download.

- [Supplementaryinformation.pdf](#)
- [1.Verocells.gif](#)
- [1.Verocells.mov](#)
- [2.BHK21hACE2cells.gif](#)
- [2.BHK21hACE2cells.mov](#)
- [3.Caco2cells.gif](#)
- [3.Caco2cells.mov](#)
- [4.Calu3cells.gif](#)
- [4.Calu3cells.mov](#)
- [5.CHOK1hACE2cells.gif](#)
- [5.CHOK1hACE2cells.mov](#)
- [6.HEK293FThACE2cells.gif](#)
- [6.HEK293FThACE2cells.mov](#)
- [7.A549hACE2cells.gif](#)
- [7.A549hACE2cells.mov](#)
- [1.Verocells.gif](#)
- [2.BHK21hACE2cells.gif](#)
- [3.Caco2cells.gif](#)
- [4.Calu3cells.gif](#)
- [5.CHOK1hACE2cells.gif](#)
- [6.HEK293FThACE2cells.gif](#)
- [7.A549hACE2cells.gif](#)
- [1.Verocells.mov](#)
- [2.BHK21hACE2cells.mov](#)
- [3.Caco2cells.mov](#)
- [4.Calu3cells.mov](#)
- [5.CHOK1hACE2cells.mov](#)
- [6.HEK293FThACE2cells.mov](#)
- [7.A549hACE2cells.mov](#)